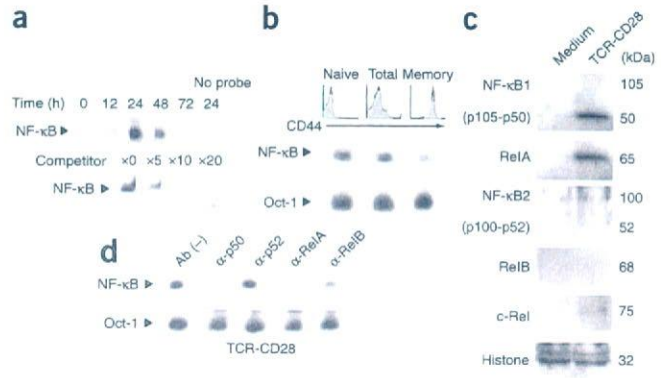

Figure 1 NF-κB activation in CD4+ T cells. (**a**) EMSA of NF-κB activity in nuclear extracts from CD4+ T cells from lymph nodes of B6 mice stimulated (times, above lanes) with crosslinked anti-TCR (1 μg/ml) and anti-CD28 (20 μg/ml). Below, EMSA with competitor (concentration, above lanes). (**b**) EMSA of NF-κB and Oct-1 activity in nuclear extracts of total, naive CD44^{lo} or memory CD44^{hi} CD4+ T cells stimulated for 24 h by TCR-CD28 ligation as in **a**. Top, CD44 expression on the cells before culture, determined by flow cytometry. (**c**) Immunoblot for NF-κB subunits in nuclear extracts of naive CD4+ T cells cultured in medium alone or activated for 24 h by TCR-CD28 ligation. (**d**) Antibody supershift assay of nuclear extracts from purified naive CD4+ T cells obtained from B6 lymph nodes; cells were stimulated for 24 h by TCR-CD28 ligation. Ab (–), no antibody; α-, antibody to. Results are representative of three to five independent experiments.

processing of p100 to p52 through IKKα both in hematopoietic cells and osteoclasts[25–27]. *Map3k14*$^{-/-}$ and aly/aly mice lack lymph nodes, and, at least for aly/aly mice, T cells show defective proliferation and IL-2 production in response to stimulation with antibody to CD3 (anti-CD3)[13,28,29]. In addition, NIK may be involved in the maintenance of central tolerance in the thymus[30]. Moreover, aly/aly mice as well as *Relb*$^{-/-}$ mice show signs of autoimmune disease[20,31,32]. Despite those findings, the mechanism for the regulation of peripheral T cell activation through NIK has not been established.

Much of the data on the function of NIK has come from studies of T cell populations that have not been separated into individual subsets based on their activation status. Expression of certain surface markers, notably CD44, distinguishes mature T cells as those that are immunologically naive (naive T cells) versus those that have been primed through contact with environmental antigens (memory T cells)[33,34]. In mice, low or intermediate expression of CD44 (CD44^{lo} or CD44^{int}) indicates a naive differentiation status, whereas CD44^{hi} cells have differentiated into memory cells. Here we examine the functions of NIK, both *in vivo* and *in vitro*, in purified subsets of naive and memory CD4+ cells.

RESULTS

NF-κB1 in CD4+ cell activation

To define the kinetics of NF-κB activation during the course of normal T cell activation, we analyzed the transcriptional activity of NF-κB in stimulated CD4+ T cells from normal C57BL/6 (B6) mice by electrophoretic mobility-shift assay (EMSA) using an NF-κB-binding DNA probe. After total CD4+ T cells were stimulated with plate-bound monoclonal antibodies (mAbs) to TCR and CD28, activation of NF-κB, measured in nuclear extracts of the cells, reached a peak after 24 h and then decreased to undetectable amounts by 72 h (**Fig. 1a**). We confirmed the specificity of NF-κB activation by using unlabeled NF-κB-binding DNA as a competitor to diminish the signal.

To determine NF-κB activation in naive and memory CD4+ T cells, we stimulated enriched subsets of normal B6 CD44^{lo} (naive) and CD44^{hi} (memory) CD4+ T cells by TCR-CD28 ligation for 24 h, followed by EMSA to detect transcriptional activity of NF-κB in the nuclear extracts; we used total CD4+ cells as a control. Nuclear translocation of NF-κB was much more prominent for naive CD4+ cells than for memory cells; in contrast, transcriptional activity of an internal control (Oct-1) was the same for both subsets of CD4+ T cells (**Fig. 1b**).

To determine the extent of nuclear translocation of individual NF-κB family members in each subset, we treated naive CD4+ T cells for 24 h with mAbs to TCR and CD28, then purified nuclear extracts and did immunoblot analysis with NF-κB protein subunit–specific antibodies. Nuclear extracts had substantial amounts of both p50 and RelA, a small amount of c-Rel protein and a conspicuous absence of p52 or RelB proteins (**Fig. 1c**). Consistent with those findings, analysis of the nuclear extracts after incubation with antibodies specific for each NF-κB protein subunit ('supershift assay') showed that the mobility shift of the NF-κB DNA probe was greatest with anti-p50 or anti-RelA but only minimal with anti-p52 or anti-RelB (**Fig. 1d**), suggesting a predominance of p50-RelA dimers. That indicated, therefore, that early activation of NF-κB in naive CD4+ cells reflects nuclear translocation of NF-κB1 (p50)–RelA, with little or no contribution from NF-κB2 (p52)–RelB.

NF-κB2 in CD4+ T cell activation

The findings reported above failed to explain the T cell defects seen in NIK-deficient aly/aly and *Relb*$^{-/-}$ mice[13,20,29]. Total CD4+ T cells have been used in studies published before; thus, it was unclear whether the abnormalities noted occur at the level of specific CD4+ T cell subsets. To examine that issue, we compared the functions of total CD4+ cells and enriched subsets of naive and memory CD4+ cells. As anticipated from prior studies[13,20,29], the proliferative responses of total CD4+ cells treated for 3 d *in vitro* with mAbs to TCR and CD28 were much lower (50–70% reduction) for *Relb*$^{-/-}$, aly/aly and *Map3k14*$^{-/-}$ mice than for heterozygous littermates or wild-type B6 mice (**Fig. 2a**). We obtained similar findings with mixed-lymphocyte reactions, in which proliferative responses were elicited by exposure to allogeneic (BALB/c) spleen cells (**Fig. 2b**). The decreased response of *Relb*$^{-/-}$, aly/aly and *Map3k14*$^{-/-}$ CD4+ cells was only mildly improved after removal of CD25+CD4+cells; that is, cells with T regulatory function (T_{reg} cells)[35–37] (**Fig. 2a–c**). That finding was unexpected because removing CD25+ T_{reg} cells from control CD4+ cell samples, thus leaving CD25−CD4+ cells, led to enhanced responses (**Fig. 2c**, left versus right). Notably, CD25+CD4+ cells are nearly all CD44^{hi}, but about 50% of CD44^{hi} cells are CD25−. In wild-type mice, CD25−CD44^{hi}CD4+ cells have little or no T regulatory function and are generally considered to be memory (or 'memory-phenotype') cells. As shown for aly/+ cells in **Figure 2c**, left, depleting normal control cell samples of both CD25+ and CD44^{hi} cells, thus leaving enriched naive CD25−CD44^{lo}CD4+ cells, led to much lower proliferative responses than those noted after removal of CD25+ cells alone. These findings indicated that in wild-type mice, total CD44^{hi} cells are a mixture of two functionally distinct populations: an inhibitory population of CD25+ T_{reg} cells, and a helper population of CD25− T memory cells, which probably release stimulatory cytokines (discussed below). The situation with respect to these cell subtypes and functions is radically different for NIK-deficient cells.

For NIK-deficient aly/aly cells, poor TCR-mediated proliferative responses were generally improved only slightly after selective removal

of $CD25^+$ cells (classical T_{reg} cells). In contrast, removal of both $CD25^+$ and $CD44^{hi}$ cells led to a substantial increase in the response; thus, the remaining $CD25^-CD44^{lo}CD4^+$ naive aly/aly T cells demonstrated a hyper-responsive proliferation compared with that of a comparable population of $CD4^+$ cells from control mice (**Fig. 2a,b,d** versus **Fig. 2d–f**). We noted the hyper-responsiveness of $CD44^{lo}CD4^+$ aly/aly cells in samples from *Map3k14*$^{-/-}$ and *Relb*$^{-/-}$ mice, and it was apparent for both mixed-lymphocyte reactions and TCR-CD28–induced proliferation (**Supplementary Fig. 1** online). We also noted hyper-responsiveness for the main subset of $CD44^{int}$ cells, which like $CD44^{lo}$ cells are considered immunologically naive (that is, they have not experienced foreign antigen stimulation; **Fig. 2f**); in contrast, $CD44^{hi}CD4^+$ cells were hypo-responsive compared with control cells (**Fig. 2g** and **Supplementary Fig. 1**). In these and all subsequent experiments, samples were enriched for 'memory' $CD44^{hi}$ cells by removal of $CD25^+$ cells (which included activated T cells as well as T_{reg} cells) and $CD62L^+$ cells.

The main conclusion from the experiments reported above is that in contrast to wild-type control cells, naive $CD4^+$ cells in NIK-deficient and *Relb*$^{-/-}$ mice are poised to hyper-respond to TCR-mediated signals and the hyper-proliferative response is 'suppressed' by $CD25^-CD44^{hi}$ memory T cells (called '$CD44^{hi}CD4^+$ memory T cells' here) when total $CD4^+$ T cells are assayed. As discussed below, the properties of $CD44^{hi}CD4^+$ memory T cells in wild-type and aly/aly mice are very different: $CD44^{hi}CD4^+$ memory T cells from wild-type mice function as helper T cells for primed naive cells, whereas $CD44^{hi}CD4^+$ memory T cells from aly/aly mice function as 'suppressor' cells.

To quantitatively evaluate the suppressor function of aly/aly $CD44^{hi}CD4^+$ memory T cells, we monitored the dilution of carboxyfluorescein diacetate succinimidyl diester (CFSE) in naive $CD44^{lo}CD4^+$ 'reporter' cells preincubated with the fluorescent dye. Early (48 h) proliferative responses of CFSE-labeled control (aly/+) $CD44^{lo}CD4^+$ cells were appreciably enhanced by the addition of a similar number (5×10^4) of syngeneic aly/+ $CD44^{hi}CD4^+$ memory T cells (**Supplementary Fig. 2** online). In contrast, the proliferation of aly/aly $CD44^{lo}CD4^+$ cells was reduced considerably by the addition of syngeneic aly/aly $CD44^{hi}CD4^+$ memory T cells (**Supplementary Fig. 2**). We obtained similar results when we incubated $CD44^{hi}CD4^+$ memory T cells from wild-type B6 or aly/aly mice (both Thy-1.2^+) with CFSE-labeled $CD44^{lo}CD4^+$ cells from B6.PL mice (Thy-1.1^+; **Supplementary Fig. 2**). For $CD44^{hi}CD4^+$ memory T cells from wild-type mice, the 'helper' effect of these cells correlated with increased IL-2 in the mixed cultures (**Supplementary Fig. 2**), presumably reflecting IL-2 synthesis by the added $CD44^{hi}CD4^+$ memory T cells. In contrast, the inhibitory influence of aly/aly $CD44^{hi}CD4^+$ memory T cells correlated with a decrease in IL-2 in the cultures (**Supplementary Fig. 2**). To directly test the function of IL-2 in this experimental situation, we added exogenous IL-2 and found that it was sufficient to overcome the inhibitory effect of adding aly/aly $CD44^{hi}CD4^+$ memory T cells (**Supplementary Fig. 2**).

Because the $CD44^{hi}CD4^+$ memory T cell samples in the experiments reported above were depleted of typical $CD25^+$ T_{reg} cells, the substantial suppressive influence of aly/aly $CD25^-CD44^{hi}CD4^+$ memory T cells was very unexpected. These cells could have had high expression of Foxp3, a transcription factor that in normal mice is selectively expressed mainly in $CD25^+$ T_{reg} cells[38–40]. That was not the case, however, as we found that Foxp3 protein was undetectable in both wild-type and aly/aly $CD25^-CD44^{hi}CD4^+$ memory T cells even after TCR stimulation (**Supplementary Fig. 3** online). Detection of Foxp3 protein was restricted to $CD25^+CD4^+$ typical T_{reg} cells, and the numbers of $Foxp3^+$ cells were much lower (70–80% reduction) for aly/aly than for wild-type, consistent with published findings[30,41].

Mechanism of suppression

The findings reported above indicated that aly/aly naive and memory T cell subsets differ considerably in their capacity to synthesize and/or use IL-2. To test that hypothesis, we evaluated both cell subsets for IL-2 synthesis and IL-2Rα (CD25) expression after TCR-CD28 ligation (**Fig. 3**). For naive $CD4^+$ T cells, there was somewhat less IL-2, as measured by enzyme-linked immunosorbent assay (ELISA), in the

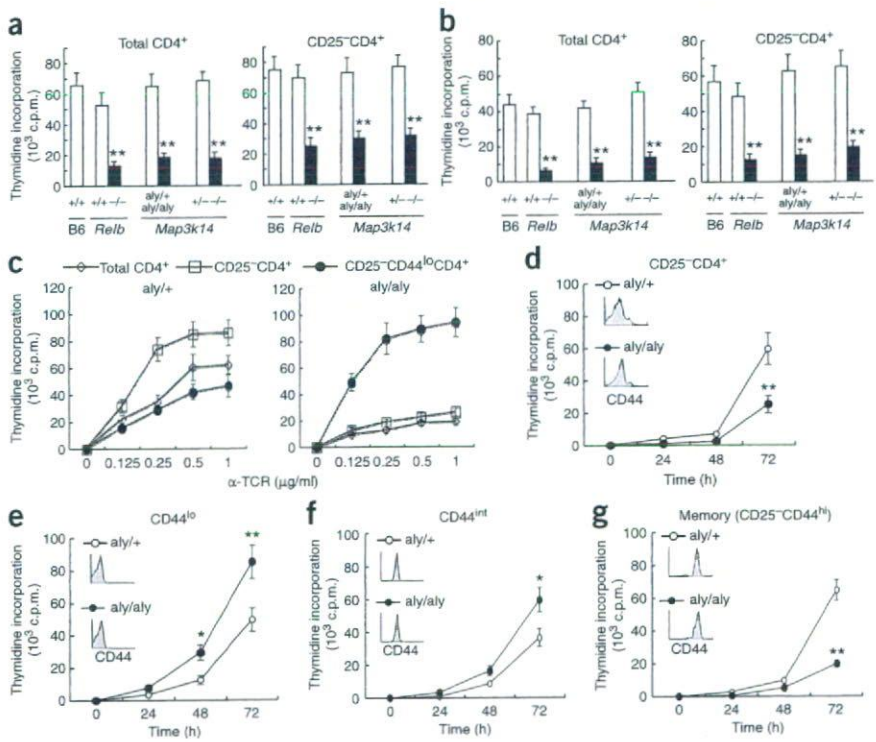

Figure 2 T cell responses of mice deficient in NF-κB2–RelB. (**a**,**b**) Proliferation assays of total $CD4^+$ and enriched $CD25^-CD4^+$ cell populations from spleens of *Relb*$^{-/-}$, aly/aly, NIK-deficient (*Map3k14*$^{-/-}$) and control (B6, *Relb*$^{+/-}$, aly/+ and *Map3k14*$^{+/-}$) mice stimulated for 72 h by TCR-CD28 ligation as in **Figure 1** (**a**) or by culture for 96 h together with irradiated T cell–depleted spleen cell samples from BALB/c mice (**b**). (**c**) Proliferation assays of total, $CD25^-$ and $CD25^-CD44^{lo}$ $CD4^+$ T cells from aly/+ and aly/aly mice; cells were stimulated for 72 h with 0–1 μg/ml (horizontal axes) of mAb to TCR (α-TCR) and 20 μg/ml of mAb to CD28. (**d**–**g**) Proliferation assays of $CD25^-CD4^+$ cells and enriched subsets of $CD44^{lo}$, $CD44^{int}$ and $CD44^{hi}$ $CD4^+$ T cells (all $CD25^-$) separated by FACSsort and stimulated for 72 h with TCR-CD28 ligation. Insets, CD44 expression on the cells before culture. *, $P < 0.05$, and **, $P < 0.005$, aly/aly mice versus control mice. Data are means ± s.d. of triplicate samples and are representative of three independent experiments.

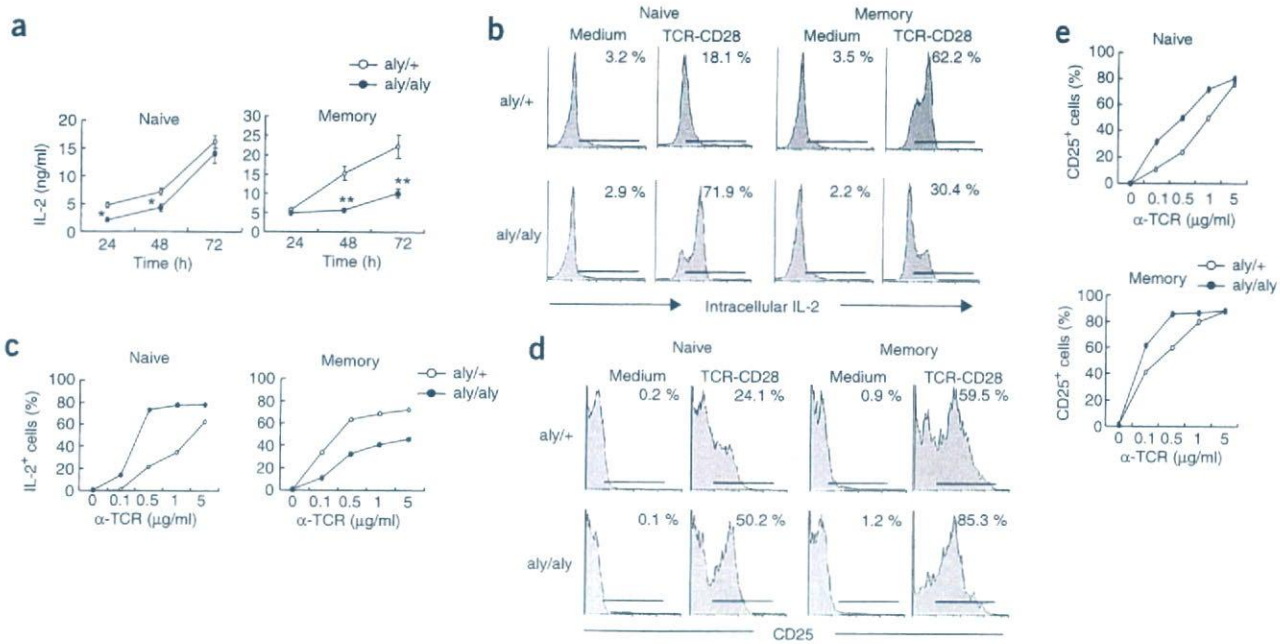

Figure 3 IL-2 secretion and IL-2R synthesis by aly/aly CD4+ subsets. (**a**) ELISA of IL-2 in culture supernatants of aly/aly and aly/+ naive CD44^{lo} and memory CD44^{hi}CD4+ T cells stimulated (time, horizontal axes) by TCR-CD28 ligation (as in **Fig. 1a**). Data are means ± s.d. of triplicate samples and are representative of four independent experiments. *, $P < 0.05$, and **, $P < 0.005$, aly/aly mice versus control mice. (**b**,**c**) Flow cytometry for intracellular IL-2 in aly/aly and aly/+ naive CD44^{lo} and memory CD44^{hi}CD4+ T cells stimulated for 24 h with mAb to TCR (0.1–5 μg/ml; horizontal axes) and mAb to CD28 (20 μg/ml; 'TCR-CD28'). (**b**) Representative data for percent IL-2+ cells (numbers above horizontal lines, in top right corners) after stimulation at 0.5 μg/ml of mAb TCR. (**c**) Mean percent of IL-2+ cells after stimulation with 'graded' concentrations of mAb to TCR. (**d**,**e**) Flow cytometry for CD25 expression on CD4+ T cells of aly/aly and aly/+ mice from **b**,**c**. (**d**) Numbers above horizontal lines indicate percent CD25+ cells after stimulation at 0.5 μg/ml of mAb TCR. (**e**) Percent CD25+ cells after stimulation with 'graded' concentrations of mAb to TCR. Results are representative of three to five independent experiments.

culture supernatants of aly/aly cells than of wild-type (aly/+) cells (**Fig. 3a**). That result was unexpected given the enhanced proliferative responses of naive aly/aly cells; however, intracellular staining showed that there was much more IL-2 protein in the cytoplasm of aly/aly cells than wild-type cells (**Fig. 3b,c**). Likewise, induction of CD25 cell surface expression was much greater on aly/aly cells than on wild-type cells (**Fig. 3d,e**). Hence, the reduced IL-2 in the culture supernatants of naive aly/aly cells presumably reflected enhanced IL-2 consumption through binding to the increased CD25 expressed on the cell surface. From these results we concluded that the increased proliferative responses of aly/aly naive cells correlated with increased IL-2 and IL-2R protein synthesis.

For CD44^{hi}CD4+ memory T cells, there was much less IL-2 synthesis in cells from aly/aly mice than in cells from control (aly/+) mice, as assessed by both the amount of IL-2 secreted into the culture supernatant (**Fig. 3a**) and the amount detected inside the cells by intracellular staining (**Fig. 3b,c**). However, the results were very different for IL-2R; compared with wild-type CD44^{hi}CD4+ memory T cells, aly/aly CD44^{hi}CD4+ memory T cells had enhanced CD25 cell surface expression, similar to that seen in the aly/aly naive cells (**Fig. 3d,e**), and the cells also demonstrated enhanced CD69 expression (data not shown). Hence, the reduced proliferative response of aly/aly CD44^{hi}CD4+ memory T cells correlated with poor IL-2 synthesis despite high IL-2R induction. The suppressive effect of aly/aly CD44^{hi}CD4+ memory T cells on naive CD4+ T cells therefore might reflect the possibility that aly/aly CD44^{hi}CD4+ memory T cells deplete the cultures of IL-2 because of enhanced expression of CD25. In agreement with that interpretation, proliferative responses of both wild-type and aly/aly naive CD4+ cells were considerably reduced by depleting the cultures of IL-2 with mAb to IL-2 (**Supplementary Fig. 2**). Moreover, in mixed cultures of naive and memory CD4+ T cells (**Supplementary Fig. 2**), poor IL-2 synthesis by these cells combined with high IL-2R expression led to IL-2 depletion, which is the likely mechanistic explanation of the suppressive property of aly/aly memory cells.

The finding that total aly/aly CD4+ cells were hyporesponsive to TCR-CD28 ligation after selective depletion of CD25+ cells suggested that the CD25+ T_{reg} cells in aly/aly mice are functionally defective. Alternatively, the aly/aly T_{reg} cells might have 'normal' suppressive activity but function poorly because their relative numbers are much lower than those in wild-type mice (**Supplementary Fig. 3**). In support of the last idea, the capacity of purified CD25+CD4+ cells to suppress proliferation of wild-type naive CD4+ T cells was almost as efficient for aly/aly CD25+ cells as it was for wild-type CD25+ cells (**Supplementary Fig. 4** online). Likewise, aly/aly and wild-type CD25+ cells were comparable in their low synthesis of IL-2 but high synthesis of both IL-10 and transforming growth factor-β (**Supplementary Fig. 4**).

In vivo responses

To examine responses *in vivo*, we first compared normal and aly/aly CD4+ subsets for their capacity to undergo homeostatic proliferation in syngeneic irradiated mice. As described before[42], the paucity of T cells in irradiated mice allows adoptively transferred CD4+ T cells to proliferate in response to major histocompatibility complex class II–restricted self peptides. Homeostatic proliferation of CFSE-labeled naive CD44^{lo}CD4+ cells was greater for aly/aly cells than for normal aly/+ cells (**Fig. 4a**). In contrast, homeostatic proliferation

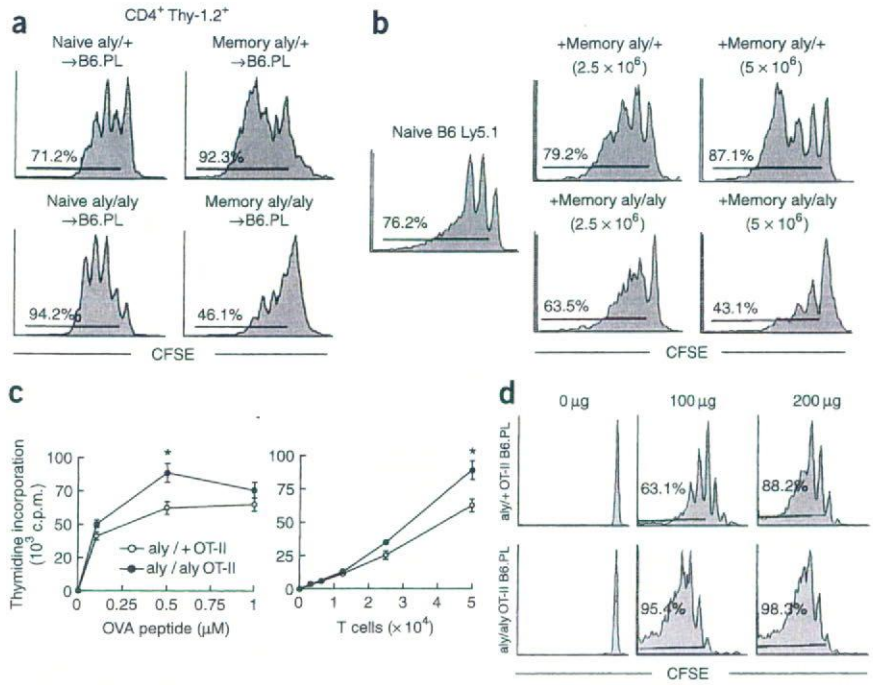

Figure 4 Proliferative responses of naive and memory aly/aly CD4+ subsets *in vivo*. (**a**) Flow cytometry of CFSE-labeled naive CD44^{lo} or memory CD44^{hi} CD4+ T cells (5 × 10^6) from aly/aly and aly/+ mice (both Thy-1.2) transferred 7 d previously into irradiated (700 rads) B6.PL (Thy-1.1) mice. (**b**) Flow cytometry of CFSE-labeled naive CD4+ T cells (5 × 10^6) from B6 Ly5.1 mice transferred together with unlabeled aly/+ or aly/aly memory cells (2.5 × 10^6 or 5 × 10^6; both Ly5.2) into irradiated (700 rads) B6 mice. Ly5.1+CD4+ T splenocytes were evaluated 7 d after transfer. (**c**) Proliferative assay of naive CD44^{lo}CD4+ T cells from either aly/aly OT-II or aly/+ OT-II mice cultured for 72 h *in vitro* with irradiated (1,500 cGy) T cell–depleted B6 spleen cell samples (5 × 10^5 cells) in the presence of 'graded' concentrations of OVA peptide (left) or with 'graded' numbers of T cells and 0.5 μM OVA peptide (right). Data are means ± s.d. of triplicate cultures. *, $P < 0.05$, aly/aly OT-II versus aly/+ OT-II cells. (**d**) Flow cytometry of CSFE-labeled naive CD4+ T cells (5 × 10^6) from aly/aly or aly/+ OT-II B6.PL mice (both Thy-1.1+) transferred intravenously into B6 (Thy-1.2+) mice; 1 d later, OVA peptide (0–200 μg) was injected intraperitoneally into recipient mice. Thy-1.1+Vβ5.2+CD4+ T splenocytes were analyzed 3 d after peptide injection. Numbers above horizontal lines (**a**,**b**,**d**) indicate percentages of divided cells from the fourth division. Results are representative of two (**b**) or three (**a**,**c**,**d**) independent experiments.

their merged fluorescence. We obtained similar results for naive aly/aly cells, although in this case the fluorescence of NF-κB1 and RelA was stronger in the nucleus than in the cytoplasm, suggesting increased nuclear translocation (**Fig. 5a**). In support of that conclusion, immunoblot analysis of nuclear extracts showed substantially more p50 and RelA in aly/aly cells than in aly/+ cells (**Fig. 5b**). In contrast, NF-κB2 and RelB were almost undetectable in the nuclei of both aly/aly and aly/+ cells, despite high expression of both proteins in the cytoplasm of aly/+ cells (**Fig. 5a**). These data confirmed that at 1 d after TCR-CD28 ligation, nuclear translocation of NF-κB was restricted mainly to NF-κB1 (p50)–RelA dimers (**Fig. 1**). There was also enhanced nuclear translocation of p50 and RelA in naive *Relb*$^{-/-}$ cells, as demonstrated by both confocal and immunoblot analyses (**Supplementary Fig. 5** online). Thus, hyper-responsiveness of naive aly/aly and *Relb*$^{-/-}$ CD4+ T cells correlated with increased nuclear translocation of NF-κB1 (p50)–RelA compared with that of wild-type naive T cells.

Through IκB-like ankyrin repeats, NF-κB2 p100 can bind other NF-κB family members and thereby prevent their nuclear translocation[3]. The hyper-responsiveness of naive aly/aly CD4+ cells, therefore, might reflect reduced p100. To test that possibility, we evaluated cytoplasmic and total cell lysates of naive aly/aly CD4+ cells; both showed a substantial reduction in p100 protein relative to that in aly/+ cells (**Fig. 5c**). We confirmed that result by fluorescence resonance energy transfer (FRET) analysis, which showed that association of p52-p100 with RelA or p50 in aly/aly cells was undetectable (**Fig. 5d**). In contrast, control naive aly/+ cells showed substantial intracytoplasmic association of p52-p100 with both RelA and p50 (**Fig. 5d**). For the control aly/+ and wild-type B6 cells, we confirmed the association of RelA and p50 with p52-p100 by immunoprecipitation of cytoplasmic extracts with anti–p52-p100 followed by immunoblot with NF-κB subunit–specific antibodies. After TCR-CD28 stimulation, p52-p100 protein (mostly p100) was associated with RelB, RelA and p50 but not with c-Rel (**Fig. 5e** and **Supplementary Fig. 5**). Also, immunoprecipitation of [^{35}S]methionine-labeled cells with anti-RelA demonstrated a notable p100-RelA complex in wild-type cells but not in aly/aly cells (**Supplementary Fig. 5**). Based on those observations, the hyper-responsiveness of naive aly/aly CD4+ cells can be attributed to reduced p100, which enhances nuclear translocation of p50-RelA and NF-κB-mediated gene transcription and cell activation.

For aly/+ CD44^{hi}CD4+ memory T cells, there was increased production and nuclear translocation of both NF-κB1 and RelA after TCR-CD28 ligation, although less than for naive aly/+ cells (**Fig. 5a**). Nuclear translocation of the alternative NF-κB2 and RelB proteins was very prominent for aly/+ CD44^{hi}CD4+ memory T cells and correlated with much more p52 in total cell lysates (**Fig. 5c**). In notable contrast, aly/aly CD44^{hi}CD4+ memory

of CD44^{hi}CD4+ memory T cells was much less for aly/aly cells than for normal aly/+ cells. Likewise, homeostatic proliferation of wild-type naive CD4+ cells (CFSE labeled) *in vivo* was enhanced by the addition of wild-type memory CD4+ cells (not CFSE labeled) but was inhibited by the addition of aly/aly CD44^{hi}CD4+ memory T cells (**Fig. 4b**). There was also hyper-responsiveness of naive aly/aly CD4+ cells *in vivo* for antigen-specific CD4+ cells. Thus, compared with control aly/+ naive OT-II cells, aly/aly naive CD44^{lo}CD4+ OT-II cells demonstrated enhanced proliferative responses to stimulation with specific ovalbumin (OVA) peptide *in vitro* (**Fig. 4c**) and to a limiting dose of OVA peptide (100 μg/mouse) *in vivo* (**Fig. 4d**).

NF-κB expression in naive versus memory CD4+ cells

To understand the hyper-responsiveness of naive aly/aly cells, it was important to determine the expression of individual NF-κB subunits in wild-type and NIK-deficient CD4+ cells. For naive CD44^{lo}CD4+ cells from control aly/+ mice, confocal microscopy after TCR-CD28 ligation for 24 h showed increased synthesis of NF-κB1 and RelA in the cytoplasm and translocation of both subunits to the nucleus (**Fig. 5a**); the two subunits were in close proximity, as indicated by

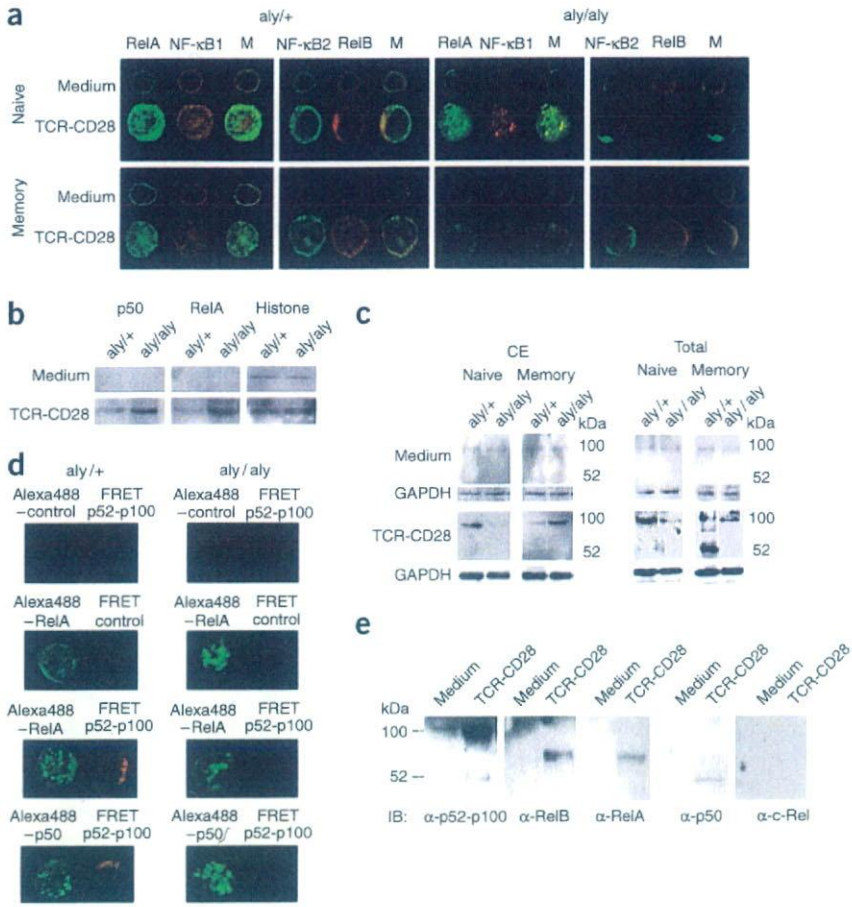

Figure 5 Molecular interactions between NF-κB subunits during T cell activation. (**a**) Confocal microscopy of naive CD44^{lo} and memory CD4$^+$ T cells from aly/aly and aly/+ mice stimulated for 24 h with TCR-CD28 ligation (as in **Fig. 1**), fixed in 3% paraformaldehyde on a glass slide and stained with anti-p50, anti-RelA, anti-p52 and anti-RelB followed by Alexa Fluor 488–labeled (green) or Alexa Fluor 568–labeled (red) anti-mouse or anti-rabbit IgG. M, merged image. Original magnification, ×630. (**b**) Immunoblot to detect p50 and RelA in nuclear extracts from naive aly/aly and aly/+ CD4$^+$ T cells after 24 h of TCR-CD28 ligation. Histone serves as a control. (**c**) Immunoblot to detect NF-κB2 (p52-p100) in total and cytosolic extracts (CE) of stimulated naive and memory CD4$^+$ T cells from aly/aly and aly/+ mice. Glyceraldehyde phosphate dehydrogenase (GAPDH) serves as a control. (**d**) FRET analysis of aly/aly and aly/+ naive CD4$^+$ T cells stimulated for 24 h with TCR-CD28 ligation, fixed in 3% paraformaldehyde on a glass slide and stained with Alexa Fluor 488–labeled (Alexa488) anti-p50 or anti-RelA and Alexa Fluor 546–labeled anti-p52. The binding of p52 to RelA or p50 is detected as a FRET signal (red). Control, no first antibody. Original magnification, ×630. (**e**) Immunoprecipitation with anti-NF-κB2 p100-p52 and immunoblot (IB) for p100-p52, RelB, p50, RelA and c-Rel in cytosolic extracts of naive B6 CD4$^+$ T cells stimulated for 24 h with TCR-CD28 ligation. Results are representative of three to five independent experiments.

T cells demonstrated no detectable nuclear translocation of RelA, NF-κB1, NF-κB2 or RelB (**Fig. 5a**). For NF-κB2, p100 was apparent in the cytoplasm of aly/aly CD44^{hi}CD4$^+$ memory T cells, as shown by both confocal microscopy (**Fig. 5a**) and immunoblot of cytoplasmic extracts (**Fig. 5c**); processing of p100 to p52 was undetectable.

Kinetics of p100 synthesis and p52 nuclear translocation

The data reported above apply to early (day-1) responses to TCR-CD28. For naive aly/aly CD4$^+$ cells, kinetics experiments showed that p100 in protein cytoplasmic extracts was undetectable for up to 72 h, which correlated with above-normal nuclear translocation of NF-κB1–p50 throughout this time (**Fig. 6a,b**). In contrast, for aly/+ naive CD4$^+$ cells, the amount of p100 in cytoplasmic extracts was high at 24 and 48 h, which correlated with only moderate amounts of NF-κB1–p50 in nuclear extracts. We also noted that nuclear p50 in aly/+ naive cells fell to undetectable amounts by 72 h and was 'replaced' by low but detectable amounts of p52-RelB. We noted the delayed nuclear translocation of p52-RelB only for aly/+ and not aly/aly cells, and this paralleled a decrease in cytoplasmic p100, perhaps reflecting p100-to-p52 processing; delayed nuclear translocation of p52-RelB in aly/+ cells was also apparent by confocal microscopy (**Fig. 6c**). These observations strengthen the view that via direct protein-protein interaction, p100 in the cytoplasm serves to inhibit nuclear translocation of p50-RelA in aly/+ naive CD4$^+$ cells and thereby acts as a 'brake' for gene transcription. The data also indicate that after several days, NF-κB activation in aly/+ naive CD4$^+$ cells involves a 'switch' from NF-κB1- to NF-κB2-dependent pathways.

Induction of autoimmune disease

NIK-deficient and *Relb*$^{-/-}$ mice develop CD4-dependent, slow-onset (>14 weeks), multiorgan autoimmune disease, which can be 'adoptively transferred' to hosts deficient in recombination-activating gene 2 (*Rag2*$^{-/-}$ hosts)[20,31,32]. Given the data reported above, autoimmune disease might be enhanced by the removal of CD44^{hi}CD4$^+$ memory T cells. To investigate that possibility, we adoptively transferred enriched subsets of aly/+ and aly/aly CD4$^+$ T cells into *Rag2*$^{-/-}$ hosts. For both control naive and memory aly/+ CD4$^+$ T cells, cell numbers recovered from the spleen after adoptive transfer were modest (about 5×10^5 cells/mouse; **Fig. 7a**), infiltration of lymphocytes in the lungs and lacrimal glands was minimal (**Fig. 7b**) and evidence of autoimmune disease in those tissues was undetectable (**Fig. 7c**). We obtained very different results after injecting aly/aly CD4$^+$ cells. For those, injection of either total CD4$^+$ or CD25$^-$CD4$^+$ cells resulted in relatively low recovery of cells from the spleen (**Fig. 7c**), thus correlating with the hyporesponsiveness of the aly/aly cells (as demonstrated above). As for autoimmune disease induction, both populations produced mild but detectable lymphocyte infiltration of lungs and lacrimal glands, with such pathology being slightly more prominent with CD25$^-$ cells (**Fig. 7b,c**). The effects were much more prominent, however, after injection of enriched naive CD4$^+$ cells (that is, samples depleted of both T_{reg} cells and memory CD4$^+$ T cells): cell recoveries were considerably enhanced in the spleen (presumably reflecting enhanced homeostatic proliferation) and there was substantial lymphocytic infiltration and prominent pathology in lung and lacrimal glands. These results demonstrated that the hyper-responsiveness of purified naive aly/aly CD4$^+$ cells applies not only to short-term proliferative

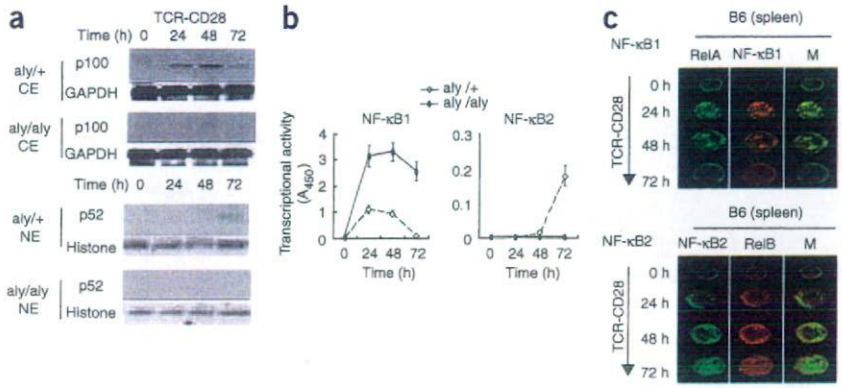

Figure 6 Kinetics of NF-κB1 and NF-κB2 expression in naive CD4$^+$ cells after TCR ligation. (**a**) Immunoblot to detect p100 and p52 in cytosolic extracts (CE) and nuclear extracts (NE) of aly/+ and aly/aly naive CD4$^+$ cells after 0–72 h of TCR-CD28 ligation. GAPDH and histone serve as controls. Results are representative of two independent experiments. (**b**) Nuclear expression of NF-κB1 and NF-κB2. Relative activities were measured with the nuclear extracts of naive T cells from aly/+ and aly/aly mice stimulated for 0–72 h with TCR-CD28 ligation. Data represent means ± s.d. of triplicate wells. (**c**) Confocal analysis of NF-κB subunits in naive CD4$^+$ cells from B6 mice stimulated for 0–72 h with TCR-CD28 and then stained with anti-p50, anti-RelA, anti-p52 and anti-RelB, followed by secondary Alexa Fluor 488–labeled (green) or Alexa Fluor 568–labeled (red) anti-mouse or anti-rabbit IgG. M, merged images. Original magnification, ×630. Results are representative of two independent experiments.

responses and related cytokine production but also to induction of autoimmune disease after transfer into *Rag2*$^{-/-}$ hosts.

DISCUSSION

For T cells, primary immune responses generally require the classical NF-κB1 pathway[43]; whether T cell activation also requires the non-classical NF-κB2 pathway is less clear. Nevertheless, studies of NIK-deficient aly/aly mice have led to the conclusion that 'optimal' activation of mature T cells requires signaling via NIK as well as PKC-θ[13]. Because NIK controls processing of p100 to p52, it would seem to follow that T cell activation is partly dependent on nonclassical NF-κB2. However, the T cell defects in aly/aly mice also correlate with reduced spleen cell expression of p50, RelA and c-Rel[13,29], suggesting an indirect effect on the classical NF-κB1 pathway.

Here we have shown that the relative contributions of NF-κB1 and NF-κB2 to T cell activation are crucially dependent on whether the cells are immunologically naive. We have made two main points in this context. The poor immune response of total aly/aly T cells (equally true for NIK-deficient *Map3k14*$^{-/-}$ and *Relb*$^{-/-}$ cells) does not reflect a positive requirement for NF-κB2 but instead reflects the inhibitory function of a unique population of 'suppressor' cells in the total cell population. However, when depleted of those suppressor cells, the aly/aly naive T cell samples showed their cell-intrinsic 'defect' of hyper-reactivity after TCR stimulation. Thus, the aly, NIK-deficient and *Relb*$^{-/-}$ phenotype is actually a combination of a cell-extrinsic suppressor function in a subset of CD44^{hi}CD4$^+$ NIK-deficient T cells and a cell-intrinsic hyperactivation response in naive CD4$^+$ T cells that lack NIK function.

For wild-type mice, it is well established that primary responses of T cells can be suppressed by a population of CD25$^+$Foxp3$^+$CD4$^+$ T_{reg} cells and are enhanced when T_{reg} cells are eliminated[38–40]. For aly/aly T cells, the enhancing effect of removing CD25$^+$CD4$^+$ T_{reg} cells was much less pronounced, probably because the proportion of the NIK-deficient CD25$^+$CD4$^+$ T_{reg} cells (specifically Foxp3$^+$ cells) is only 20–30% of the number of such cells in wild-type mice. However, the aly/aly CD25$^+$CD4$^+$ T_{reg} cells are suppressor cells functionally, as after enrichment they suppressed the proliferation of naive T cells nearly as well as T_{reg} cells from control mice. In addition, cytokine production by T_{reg} cells from aly/aly and control mice was comparable. Hence, except for an overall reduction in

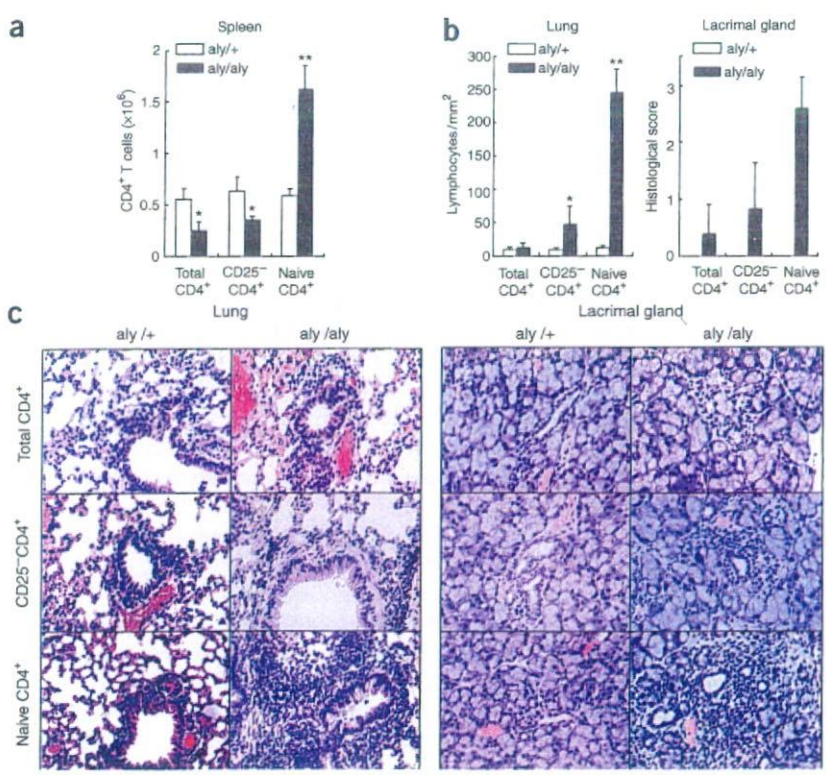

Figure 7 Induction of autoimmune disease by subsets of aly/+ and aly/aly CD4$^+$ cells. Enriched subsets of total CD4$^+$, CD25$^-$CD4$^+$ or naive (CD25$^-$CD44^{lo}) CD4$^+$ cells from aly/+ and aly/aly mice were transferred into *Rag2*$^{-/-}$ hosts (5×10^6 cells/mouse); mice were killed 4 weeks after transfer. (**a**) Total number of CD3$^+$CD4$^+$ splenocytes. Data are means ± s.d of four to five mice. *, $P < 0.05$, and **, $P < 0.005$, aly/aly versus aly/+ cells in each group. (**b**) Histopathological analysis of lung and lacrimal gland sections. Left, number of lymphocytes/mm^2 of lung; right, pathological score of inflammatory lesions of lacrimal glands. Data are means ± s.d. of four to five mice. (**c**) Histology of lungs and lacrimal gland sections stained with hematoxylin and eosin. Original magnification, ×100. Results are representative of four to five mice in each group.

total numbers, the 'classical' $CD25^+CD4^+$ T_{reg} cells in aly/aly mice showed no obvious abnormality.

The situation with memory $CD4^+$ cells was very different. Wild-type memory $CD25^-CD44^{hi}CD4^+$ T cells functioned like 'typical' antigen-primed T cells: they rapidly generated large amounts of IL-2 after TCR ligation *in vitro* and provided efficient help to naive $CD4^+$ T cells. In contrast, all of the data presented here indicate the conclusion that aly/aly memory $CD4^+$ T cells function as suppressor cells. In every test, both *in vivo* and *in vitro*, elimination of both $CD25^+$ ('typical' T_{reg} cells) and $CD25^-CD44^{hi}CD4^+$ memory T cells was required for reversal of the poor proliferative response of aly/aly $CD4^+$ cells. The origin of such 'naturally' occurring $CD44^{hi}CD4^+$ memory cells in either wild-type or NIK-deficient mice is unclear; such cells may arise through contact with various environmental antigens and/or be stimulated by self antigens.

The mechanism of suppression by aly/aly memory $CD4^+$ cells has yet to be resolved. After TCR ligation, suppression correlated with a combination of low IL-2 synthesis and enhanced CD25 expression, which suggests that the cells could function mostly through CD25-mediated consumption of IL-2. That idea fits with the finding that suppression by aly/aly memory $CD4^+$ T cells *in vitro* could be overcome by the addition of exogenous IL-2. However, simple consumption of IL-2 is unlikely to explain the strong inhibitory influence of aly/aly memory $CD4^+$ T cells *in vivo*, which was apparent for both homeostatic proliferation and autoimmune disease induction. By analogy with 'typical' T_{reg} cells, suppression via transforming growth factor-β or IL-10 production could be involved[35–37]; however, at least *in vitro*, production of these cytokines was no higher for aly/aly memory $CD4^+$ T cells than for control memory cells. Hence, resolving the mechanisms of suppression by aly/aly memory $CD4^+$ cells must await further investigation.

Why memory $CD4^+$ cells in aly/aly mice show strong CD25 expression but poor IL-2 synthesis after TCR stimulation is also still unclear. Nevertheless, it is notable that despite enhanced synthesis of CD25, aly/aly memory $CD4^+$ T cells demonstrated very little nuclear translocation of p50, RelA, p52, RelB (as presented here) or c-Rel (data not shown), indicating that CD25 upregulation in aly/aly memory cells involves an NF-κB-independent pathway, such as AP-1 and/or NF-AT[44,45]. Because nuclear translocation of p50-RelA was high in naive aly/aly T cells, the limited translocation of these subunits in memory aly/aly T cells in comparison was unexpected although consistent with the reduced p50 and RelA reported for aly/aly total spleen cells[29]. Based on those preliminary data, poor nuclear translocation of p50 and RelA in memory aly/aly $CD4^+$ cells correlates with reduced synthesis in the cytoplasm, suggesting that p50 and RelA synthesis in memory $CD4^+$ cells is partly controlled by a NIK-dependent pathway. In addition, as in stimulated osteoclast precursors[26], the low amounts of p50 and RelA in aly/aly memory $CD4^+$ cells may be 'held' in the cytoplasm through association with p100; thus, cytoplasmic p100 in aly/aly cells is much higher in memory cells than naive cells.

The hyper-responsiveness of naive aly/aly $CD4^+$ cells was associated with increased synthesis of both IL-2R (CD25) and IL-2, relative to that of wild-type naive cells; detection of an increase in IL-2 synthesis required intracellular staining, presumably because of efficient absorption of extracellular IL-2 by the increased CD25 expressed on the cell surface. Other signs of T cell activation, such as CD69 expression and interferon-γ synthesis, were nearly normal (data not shown), indicating that the hyper-responsiveness was centered on the IL-2–IL-2R axis. As for NF-κB, it is particularly notable that the increased proliferative responses of naive aly/aly $CD4^+$ cells were associated with considerable increases in nuclear translocation of p50 and RelA, apparent in both nuclear extracts and by confocal microscopy. Therefore, this indicates that NIK functions by preventing nuclear translocation of p50 and RelA. The simplest possibility is that NIK regulates autocrine synthesis of p100 through continuous p100-p52 processing, thus allowing nuclear translocation of p52-RelB dimers and transcription of the gene encoding p100 (ref. 26); steady-state production of p100 then keeps p50 and RelA in the cytoplasm. We favor that hypothesis because there was much less p100 in aly/aly naive cells than in control cells; that result was also confirmed by FRET analysis, which showed no apparent association of p100 with p50 or RelA. Hence, we attribute the hyper-responsiveness of aly/aly naive $CD4^+$ cells (as well as *Map3k14*$^{-/-}$ (NIK-deficient) and *Relb*$^{-/-}$ cells) to reduced p100 synthesis, which leads to unregulated nuclear translocation of p50-RelA and enhanced IL-2 and IL-2R synthesis. For *Relb*$^{-/-}$ cells, p100 was also reduced (data not shown), presumably because expression of the gene encoding autocrine p100 is controlled by p52-RelB heterodimers[26].

For naive $CD4^+$ cells from wild-type mice, despite prominent synthesis in the cytoplasm, nuclear translocation of p52-RelB was undetectable within the first 2 d after TCR-CD28–induced activation, indicating no involvement of the nonclassical NF-κB2 pathway. However, by day 3 after TCR ligation, substantial nuclear translocation of p52-RelB was evident, which paralleled a decrease in p50-RelA. That result provides direct support for the hypothesis that NF-κB2–RelB is involved in the later stages of the primary response[46–48], perhaps by 'substituting' for the classical NF-κB1 pathway. One point to emphasize here is that nuclear translocation of NF-κB2–RelB presumably has only a positive effect on gene transcription and thus cannot account for the regulatory effect of NIK on TCR responsiveness. As mentioned above, we envisage that NIK acts as a 'brake' for the NF-κB1 pathway simply by maintaining unprocessed p100 in the cytoplasm, thereby impeding entry of p50-RelA into the nucleus.

In summary, our data here have shown that the T cell defects reported for NIK-deficient mice[13] and *Relb*$^{-/-}$ mice[20] reflect a dominant form of immunoregulation in which otherwise hyper-responsive NIK-deficient naive T cells are suppressed by a subset of NIK-deficient $CD25^-$ memory T cells. Only when the suppressor cells are eliminated is the cell-intrinsic phenotype of NIK-deficiency demonstrated. At face value, these results may seem at odds with the observation that aly/aly mice develop multiorgan autoimmune disease. That syndrome, associated with a reduction in classic $CD25^+$ T_{reg} cells, may be triggered by poor negative selection in the thymus because of reduced expression of various self antigens in the thymic medulla[30]. Given such a self-tolerance defect, it is unexpected that autoimmune disease in aly/aly mice is relatively mild, which suggests that the 'nontolerant' T cells in these mice are generally very well controlled, perhaps by the inhibitory memory subset we have described here. The fulminating autoimmune disease seen when purified naive aly/aly $CD4^+$ cells were transferred adoptively is consistent with that idea.

METHODS

Mice. B6 and 129 mice were obtained from the Jackson Laboratory. *Map3k14*$^{-/-}$ (NIK-deficient), *Map3k14*$^{aly/aly}$ (aly/aly) and *Relb*$^{-/-}$ mice were provided by R. Ulevitch (The Scripps Research Institute, La Jolla, California) and M. Kronenberg (La Jolla Institute for Allergy and Immunology, San Diego, California), and OT-II mice[49] (C57BL/6-Tg(TcraTcrb)425Cbn/J) were obtained from S. Webb (The Scripps Research Institute, La Jolla, California); aly/aly OT-II mice were generated by crossing of aly/aly mice with OT-II mice. *Rag2*$^{-/-}$ mice were obtained from Taconic. All mice were maintained in specific pathogen–free conditions in our animal facility and the experiments were approved by an animal ethics board of The Scripps Research Institute (La Jolla, California) or Tokushima University (Tokushima, Japan).

Antibodies. Antibodies specific for p50 (C-19, NLS and D-17), p52 (K-27 and C-5), RelA (A-20, C-20 and F-6), RelB (C-19), c-Rel, histone and glyceraldehyde phosphate dehydrogenase were purchased from Santa Cruz Biotechnology and were used for immunoprecipitation, immunoblot analysis, EMSA and confocal microscopy.

Cell purification. For purification of $CD4^+$ subsets, lymph node or spleen cells were treated for 45 min at 37 °C with cytotoxic mAbs specific for CD8 (3.168.8) and CD24 (J11D) plus guinea pig complement (Rockland)[50]. After being washed, $CD25^+CD4^+$ T cells, $NK1.1^+$ T cells and cells positive for major histocompatibility complex class II first underwent depletion by negative selection with DynaBeads (Dynal). Samples were enriched for $CD44^{lo}$ and $CD44^{hi}$ cells by negative selection with anti-CD44 (IM7) or anti-CD62L (Mel-14) and were positively 'panned' with anti-CD4 (RL172). In addition, samples were enriched for $CD44^{lo}$, $CD44^{int}$ and $CD44^{hi}$ $CD4^+$ and $CD25^+CD4^+$ T cells by cell sorting with a FACSvantage (Becton Dickinson).

Culture conditions. Cells were cultured in 0.2 ml of RPMI medium supplemented with 50 μM 2-mercaptoethanol, L-glutamine and 10% FCS in 96-well tissue culture plates coated with mAbs specific for TCRβ (H57-597) and CD28 (37.51; eBiosciences).

Flow cytometry. A FACSsort (Becton Dickinson) was used for flow cytometry and data were analyzed with FlowJo FACS Analysis software (Tree Star). Analysis of cell division with CFSE (Molecular Probes)[42], intracellular cytokine production (IL-2) with a BD Cytofix/Cytoperm kit (BD Biosciences)[51] and intracellular Foxp3 expression with an Intracellular Foxp3 Detection Kit (eBioscience) was done according to the manufacturers' instructions.

Proliferation assay. Cell proliferation was evaluated by [^{3}H]thymidine incorporation or by counting of divisions by CFSE dilution of labeled cells. In most experiments, 5×10^4 enriched $CD4^+$ T cells were stimulated for 24–72 h with plate-bound mAbs to TCR (0.1-1 μg/ml) and CD28 (20 μg/ml). OT-II T cells (0.625×10^4 to 5×10^4 cells/well) were cultured together with irradiated (3,000 cGy) Thy-1.2^+-depleted syngeneic spleen cell samples (5×10^5 cells) and were stimulated with OVA peptide, amino acids 323–339 (Sigma Genosys). Stimulated cells were then pulsed with 0.5 μCi [^{3}H]thymidine per well for the last 8 h of culture. For CFSE labeling, purified $CD4^+$ T cells were resuspended with 0.1% BSA in PBS at a density of 5×10^6 cells/ml and were labeled for 10 min at 37 °C with 0.3 μM CFSE. CFSE-labeled cells were 'quenched' with PBS containing 5% FCS and were washed twice. Cell division at 48–72 h was analyzed by flow cytometry.

EMSA. Nuclear extracts of stimulated $CD4^+$ T cells were prepared as described[52]. Cells were washed twice with PBS and were resuspended in 100 μl ice-cold lysis buffer, were vortexed and were centrifuged for 5 min at 5,000*g*. Nuclear pellets were resuspended in 100 μl extraction buffer containing 20 mM HEPES, 1.5 mM $MgCl_2$, 0.2 mM EDTA, 0.4 mM NaCl, 2.5% glycerol and a mixture of protease inhibitors. After centrifugation for 30 min at 12,000*g*, nuclear extracts (0.5–5 μg) in the supernatant were incubated for 20 min at 25 °C with biotin-labeled κB oligonucleotide probe (5′-AGTTGAGGG GACTTTCCCAGGC-3′) and Oct-1 oligonucleotide probe (5′-TGTCGAATG CAAATCACTAGAA-3′). Protein-DNA complexes were resolved by nondenaturing 4–6% PAGE in 0.5× TBE and were transferred to nylon membranes (Pierce). After crosslinking of transferred DNA to the membranes, biotin-labeled DNA was detected with a LightShift Chemiluminescent EMSA Kit (Pierce) according to the manufacturer's instructions. For supershift assay, NF-κB subunit–specific antibodies were added before the formation of DNA-protein complexes at 25 °C for 15 min.

Immunoprecipitation and immunoblot analysis. Nuclear extracts, cytoplasmic extracts and total cell lysates from $CD4^+$ T cells (2.5–10 μg) were separated by 10% SDS-PAGE and were blotted onto polyvinyldifluoride membranes. Blotted membranes were incubated with antibodies specific for NF-κB subunits, followed by incubation with goat anti-mouse, or donkey anti-rabbit coupled to horseradish peroxidase, and proteins were made visible with the SuperSignal West Pico Chemiluminescent Substrate (Pierce). For immunoprecipitation, purified proteins (10–50 μg) 'captured' with the antibody were incubated with immobilized protein G and were precipitated with a Seize Classic Mammalian Immunoprecipitation Kit (Pierce). Precipitated proteins were analyzed by immunoblot with the NF-κB subunit–specific antibodies described above and a Rabbit IgG TrueBlot set (eBioscience). Positive controls for the detection of NF-κB subunits were confirmed by immunoblot analysis (**Supplementary Fig. 6** online) using Jurkat or A431 cell lysates (BD Transduction Laboratories).

ELISA. The amount of IL-2 and IL-10 proteins in culture supernatants was determined by ELISA. Production of transforming growth factor-β was measured with the DuoSet ELISA Development System (R&D Systems). For this, 96-well flat-bottomed plates were precoated with capture antibodies, and diluted samples or standard recombinant cytokines were added to each well. After plates were washed, biotinylated antibodies were added and then wells were incubated with horseradish peroxidase–labeled, affinity-purified anti-rat immunoglobulin G (IgG). A solution of *o*-phenylendiamine (Sigma) was added to each well as a substrate. The optical density at 490 nm was measured with a microplate reader (Molecular Devices).

Confocal microscopy. Cells were deposited onto poly-L-lysine-coated glass slides, were fixed with 3% paraformaldehyde in PBS, were made permeable for 2 min with 0.2% Triton X-100 in PBS and were preblocked for 1 h with 1% BSA and 2.5% FCS in PBS. Cells were stained for 1 h with 1 μg/ml of the appropriate primary antibodies. After being washed three times with 0.0001% Triton X-100 in PBS, cells were stained for 30 min with secondary Alexa Fluor 488–conjugated donkey anti-mouse or goat anti-rabbit IgG (heavy plus light) and then were washed with PBS. Coverslips were applied with Fluoromount-G (Molecular Probes). Cells were visualized with a BioRad 1024 laser-scanning confocal microscope (BioRad Laboratories). Each optical section was acquired sequentially with 488-nm and 568-nm laser lines to excite Alexa Fluor 488 (green) and Alexa Fluor 568 (red) fluorescence, respectively. Merged images are presented as yellow. For FRET, Zenon Rabbit IgG Labeling Kits or Zenon Mouse IgG Labeling Kits (Molecular Probe) were used to label antibodies with Alexa Fluor 488 as the 'donor dye' or Alexa Fluor 546 as the 'acceptor dye'[53]. Red color indicates that the acceptor dye was activated by the donor dye, as the two dyes were in close proximity.

NF-κB transcription activity assay. The transcriptional activity of NF-κB subunits of the nuclear extracts from naive T cells was analyzed with NF-κB Family Transcription Factor Assay Kit (Chemicon). Nuclear extracts were incubated with biotinylated double-stranded oligonucleotide probe containing the consensus sequence (5′-GGGACTTTCC-3′) for NF-κB on a streptavidin-coated plate. Captured complexes, including active NF-κB protein, were incubated with the primary antibody for NF-κB subunit and horseradish peroxidase–conjugated secondary antibody and tetramethylbenzidine substrate. The absorbance of the samples was measured with a spectrophotometry microplate reader set at 450 nm.

Pulse-chase assay. Purified naive $CD4^+$ T cells from aly/+ and aly/aly mice were cultured for 4 h in methionine-free RPMI 1640 medium (Sigma) supplemented with ^{35}S-labeled methionine (50 μCi/ml) on plates coated with mAbs to TCR and CD28. Purified total extracts were immunoprecipitated with rabbit anti-RelA. Radiolabeled proteins in the immunoprecipitate were resolved by reduced SDS-PAGE; the dried gel was exposed to autoradiography film in a phosphorimaging cassette.

Cell transfer. CFSE-labeled naive or memory $CD4^+$ T cells (5×10^6) from aly/aly, aly/+ or B6.Ly5.1 mice were transferred intravenously into irradiated (700 cGy) B6.PL (Thy-1.1^+) or B6 mice. On day 7 after transfer, spleen cells were analyzed to measure homeostatic proliferation via CFSE dilution by flow cytometry. For analysis of *in vivo* antigen-specific T cell responses, 5×10^6 CFSE-labeled naive $CD4^+$ T cells from aly/aly OT-II B6.PL and aly/+ OT-II B6.PL mice were transferred intravenously into B6 mice; OVA peptide of amino acids 323–339 (0–200 μg) was injected intraperitoneally into the mice; 3 d later, proliferation of the donor cells in spleen and lymph node was analyzed by flow cytometry. For induction of autoimmune lesions in aly/aly mice, 5×10^6 enriched total $CD4^+$, $CD25^-CD4^+$ or naive $CD4^+$ cells from aly/+ or aly/aly mice were transferred intravenously into *Rag2*$^{-/-}$ mice.

Histological analysis. All organs of *Rag2*$^{-/-}$ mice that had received cell transfer were removed, were fixed with 4% phosphate-buffered formaldehyde, pH 7.2, and were prepared for histological examination. Sections were stained with hematoxylin and eosin. The disease incidence and severity in pancreata and lacrimal glands was determined by the histological score of inflammatory lesions as described[54]. For the inflammatory lesions of lungs, lymphocytes per mm^2 were counted. Histological findings were estimated by three independent, well-trained pathologists 'blinded' to sample identity.

Statistics. Student's *t*-test was used for statistical analyses.

Note: Supplementary information is available on the Nature Immunology website.

ACKNOWLEDGMENTS

We thank B. Marchand for typing the manuscript. Supported by the United States Public Health Service (CA38355, AI21487, AI46710 and AG01743; publication number 17327-IMM from The Scripps Research Institute) and by the Ministry of Education, Science, and Culture of Japan (grants-in-aid for scientific research; 17689049).

COMPETING INTERESTS STATEMENT

The authors declare that they have no competing financial interests.

Published online at http://www.nature.com/natureimmunology/
Reprints and permissions information is available online at http://npg.nature.com/reprintsandpermissions/

1. Ghosh, S., May, M.J. & Kopp, E.B. NF-κB and Rel proteins: evolutionarily conserved mediators of immune responses. *Annu. Rev. Immunol.* **16**, 225–260 (1998).
2. Karin, M. How NF-κB is activated: the role of the IκB kinase (IKK) complex. *Oncogene* **18**, 6867–6874 (1999).
3. Bonizzi, G. & Karin, M. The two NF-κB activation pathways and their role in innate and adaptive immunity. *Trends Immunol.* **25**, 280–288 (2004).
4. Kahn-Perles, B., Lipcey, C., Lecine, P., Olive, D. & Imbert, J. Temporal and subunit-specific modulations of the Rel/NF-κB transcription factors through CD28 costimulation. *J. Biol. Chem.* **272**, 21774–21783 (1997).
5. Sun, Z. *et al.* PKC-theta is required for TCR-induced NF-κB activation in mature but not immature T lymphocytes. *Nature* **404**, 402–407 (2000).
6. Ruland, J. *et al.* Bcl10 is a positive regulator of antigen receptor-induced activation of NF-κB and neural tube closure. *Cell* **104**, 33–42 (2001).
7. Thome, M. & Tschopp, J. TCR-induced NF-κB activation: a crucial role for Carma1, Bcl10 and MALT1. *Trends Immunol.* **24**, 419–424 (2003).
8. Karin, M. & Ben-Neriah, Y. Phosphorylation meets ubiquitination: the control of NF-κB activity. *Annu. Rev. Immunol.* **18**, 621–663 (2000).
9. Pimentel-Muinos, F. *et al.* Regulation of interleukin-2α chain expression and nuclear factor κB activation by protein kinase C in T lymphocytes. Autocrine role of tumor necrosis factor α. *J. Biol. Chem.* **269**, 24424–24429 (1994).
10. Prasad, A.S. *et al.* Zinc enhances the expression of interleukin-2 and interleukin-2 receptors in HUT-78 cells by way of NF-κB activation. *J. Lab. Clin. Med.* **140**, 272–289 (2002).
11. Dejardin, E. *et al.* The lymphotoxin-β receptor induces different patterns of gene expression via two NF-κB pathways. *Immunity* **17**, 525–535 (2002).
12. Matsushima, A. *et al.* Essential role of nuclear factor (NF)-κB-inducing kinase and inhibitor of κB (IκB) kinase α in NF-κB activation through lymphotoxin β receptor, but not through tumor necrosis factor receptor I. *J. Exp. Med.* **193**, 631–636 (2001).
13. Matsumoto, M. *et al.* Essential role of NF-κB-inducing kinase in T cell activation through the TCR/CD3 pathway. *J. Immunol.* **169**, 1151–1158 (2002).
14. Artis, D. *et al.* NF-κB1 is required for optimal CD4$^+$ Th1 cell development and resistance to *Leishmania major*. *J. Immunol.* **170**, 1995–2003 (2003).
15. Erdman, S., Fox, J.G., Dangler, C.A., Feldman, D. & Horwitz, B.H. Typhlocolitis in NF-κB-deficient mice. *J. Immunol.* **166**, 1443–1447 (2001).
16. Hilliard, B., Samoilova, E.B., Liu, T.S., Rostami, A. & Chen, Y. Experimental autoimmune encephalomyelitis in NF-κB-deficient mice:roles of NF-κB in the activation and differentiation of autoreactive T cells. *J. Immunol.* **163**, 2937–2943 (1999).
17. Das, J. *et al.* A critical role for NF-κB in GATA3 expression and T_H2 differentiation in allergic airway inflammation. *Nat. Immunol.* **2**, 45–50 (2001).
18. Beg, A.A., Sha, W.C., Bronson, R.T., Ghosh, S. & Baltimore, D. Embryonic lethality and liver degeneration in mice lacking the RelA component of NF-κB. *Nature* **376**, 167–170 (1995).
19. Burkly, L. *et al.* Expression of RelB is required for the development of thymic medulla and dendritic cells. *Nature* **373**, 531–536 (1995).
20. Weih, F. *et al.* Multiorgan inflammation and hematopoietic abnormalities in mice with a targeted disruption of RelB, a member of the NF-κB/Rel family. *Cell* **80**, 331–340 (1995).
21. Franzoso, G. *et al.* Mice deficient in nuclear factor (NF)-κB/p52 present with defects in humoral responses, germinal center reactions, and splenic microarchitecture. *J. Exp. Med.* **187**, 147–159 (1998).
22. Speirs, K., Lieberman, L., Caamano, J., Hunter, C.A. & Scott, P. Cutting edge: NF-κB2 is a negative regulator of dendritic cell function. *J. Immunol.* **172**, 752–756 (2004).
23. Hilliard, B.A. *et al.* Critical roles of c-Rel in autoimmune inflammation and helper T cell differentiation. *J. Clin. Invest.* **110**, 843–850 (2002).
24. Kontgen, F. *et al.* Mice lacking the c-rel proto-oncogene exhibit defects in lymphocyte proliferation, humoral immunity, and interleukin-2 expression. *Genes Dev.* **9**, 1965–1977 (1995).
25. Shinkura, R. *et al.* Alymphoplasia is caused by a point mutation in the mouse gene encoding Nf-κB-inducing kinase. *Nat. Genet.* **22**, 74–77 (1999).
26. Novack, D.V. *et al.* The IκB function of NF-κB2 p100 controls stimulated osteoclastogenesis. *J. Exp. Med.* **198**, 771–781 (2003).
27. Yin, L. *et al.* Defective lymphotoxin-β receptor-induced NF-κB transcriptional activity in NIK-deficient mice. *Science* **291**, 2162–2165 (2001).
28. Fagarasan, S. *et al.* Alymphoplasia (aly)-type nuclear factor κB-inducing kinase (NIK) causes defects in secondary lymphoid tissue chemokine receptor signaling and homing of peritoneal cells to the gut-associated lymphatic tissue system. *J. Exp. Med.* **191**, 1477–1486 (2000).
29. Yamada, T. *et al.* Abnormal immune function of hemopoietic cells from alymphoplasia (aly) mice, a natural strain with mutant NF-κB-inducing kinase. *J. Immunol.* **165**, 804–812 (2000).
30. Kajiura, F. *et al.* NF-κB-inducing kinase establishes self-tolerance in a thymic stroma-dependent manner. *J. Immunol.* **172**, 2067–2075 (2004).
31. Weih, F. *et al.* Both multiorgan inflammation and myeloid hyperplasia in RelB-deficient mice are T cell dependent. *J. Immunol.* **157**, 3974–3979 (1996).
32. Tsubata, R. *et al.* Autoimmune disease of exocrine organs in immunodeficient alymphoplasia mice: a spontaneous model for Sjogren's syndrome. *Eur. J. Immunol.* **26**, 2742–2748 (1996).
33. Dutton, R.W., Bradley, L.M. & Swain, S.L. T cell memory. *Annu. Rev. Immunol.* **16**, 201–223 (1998).
34. Sprent, J. & Surh, C.D. T cell memory. *Annu. Rev. Immunol.* **20**, 551–579 (2002).
35. Sakaguchi, S. Naturally arising CD4$^+$ regulatory T cells for immunologic self-tolerance and negative control of immune responses. *Annu. Rev. Immunol.* **22**, 531–562 (2004).
36. Fehervari, Z. & Sakaguchi, S. Development and function of CD25$^+$CD4$^+$ regulatory T cells. *Curr. Opin. Immunol.* **16**, 203–208 (2004).
37. Piccirillo, C.A. & Shevach, E.M. Naturally-occurring CD4$^+$CD25$^+$ immunoregulatory T cells: central players in the arena of peripheral tolerance. *Semin. Immunol.* **16**, 81–88 (2004).
38. Khattri, R., Cox, T., Yasayko, S.A. & Ramsdell, F. An essential role for Scurfin in CD4$^+$CD25$^+$ T regulatory cells. *Nat. Immunol.* **4**, 337–342 (2003).
39. Fontenot, J.D., Gavin, M.A. & Rudensky, A.Y. Foxp3 programs the development and function of CD4$^+$CD25$^+$ regulatory T cells. *Nat. Immunol.* **4**, 330–336 (2003).
40. Hori, S., Nomura, T. & Sakaguchi, S. Control of regulatory T cell development by the transcription factor Foxp3. *Science* **299**, 1057–1061 (2003).
41. Lu, L.F., Gondek, D.C., Scott, Z.A. & Noelle, R.J. NF κB-inducing kinase deficiency results in the development of a subset of regulatory T cells, which shows a hyperproliferative activity upon glucocorticoid-induced TNF receptor family-related gene stimulation. *J. Immunol.* **175**, 1651–1657 (2005).
42. Ernst, B., Lee, D-S., Chang, J., Sprent, J. & Surh, C.D. The peptide ligands mediating positive selection in the thymus control T cell survival and homeostatic proliferation in the periphery. *Immunity* **11**, 173–181 (1999).
43. Weil, R. & Israel, A. T-cell-receptor- and B-cell-receptor-mediated activation of NF-κB in lymphocytes. *Curr. Opin. Immunol.* **16**, 374–381 (2004).
44. Kim, H.P. & Leonard, W.J. The basis for TCR-mediated regulation of the IL-2 receptor α chain gene: role of widely separated regulatory elements. *EMBO J.* **21**, 3051–3059 (2002).
45. Schuh, K. *et al.* The interleukin 2 receptor α chain/CD25 promoter is a target for nuclear factor of activated T cells. *J. Exp. Med.* **188**, 1369–1373 (1998).
46. Bren, G.D. *et al.* Transcription of the RelB gene is regulated by NF-κB. *Oncogene* **20**, 7722–7733 (2001).
47. Olashaw, N.E. Inducible activation of RelB in fibroblasts. *J. Biol. Chem.* **271**, 30307–30310 (1996).
48. Ivanov, V.N., Deng, G., Podack, E.R. & Malek, T.R. Pleiotropic effects of Bcl-2 on transcription factors in T cells: potential role of NF-κB p50-p50 for the anti-apoptotic function of Bcl-2. *Int. Immunol.* **7**, 1709–1720 (1995).
49. Robertson, J.M., Jensen, P.E. & Evavold, B.D. DO11.10 and OT-II T cells recognize a C-terminal ovalbumin 323–339 epitope. *J. Immunol.* **164**, 4706–4712 (2000).
50. Kishimoto, H. & Sprent, J. Strong TCR ligation without costimulation causes rapid onset of Fas-dependent apoptosis of naive murine CD4$^+$ T cells. *J. Immunol.* **163**, 1817–1826 (1999).
51. Assenmacher, M., Schmitz, J. & Radbruch, A. Flow cytometric determination of cytokines in activated murine T helper lymphocytes: expression of interleukin-10 in interferon-γ and in interleukin-4-expressing cells. *Eur. J. Immunol.* **24**, 1097–1101 (1994).
52. Grundstrom, S., Anderson, P., Scheipers, P. & Sundstedt, A. Bcl-3 and NFκB p50-p50 homodimers act as transcriptional repressors in tolerant CD4$^+$ T cells. *J. Biol. Chem.* **279**, 8460–8468 (2004).
53. Zal, T. & Gascoigne, N.R. Using live FRET imaging to reveal early protein-protein interactions during T cell activation. *Curr. Opin. Immunol.* **16**, 418–427 (2004).
54. Ishimaru, N. *et al.* Development of autoimmune exocrinopathy resembling Sjogren's syndrome in estrogen-deficient mice of healthy background. *Am. J. Pathol.* **163**, 1481–1490 (2003).

MOLECULAR AND CELLULAR BIOLOGY, Apr. 2006, p. 2924–2935
0270-7306/06/$08.00+0 doi:10.1128/MCB.26.8.2924–2935.2006

Vol. 26, No. 8

Novel Role for RbAp48 in Tissue-Specific, Estrogen Deficiency-Dependent Apoptosis in the Exocrine Glands

Naozumi Ishimaru,[1] Rieko Arakaki,[1] Fumie Omotehara,[1] Koichi Yamada,[2] Kenji Mishima,[2] Ichiro Saito,[2] and Yoshio Hayashi[1]*

Department of Oral Molecular Pathology, Institute of Health Biosciences, The University of Tokushima Graduate School, 3 Kuramotocho, Tokushima 770-8504,[1] and Department of Pathology, Tsurumi University School of Dentistry, Tsurumi,[2] Japan

Received 1 August 2005/Returned for modification 31 August 2005/Accepted 20 January 2006

Although tissue-specific apoptosis in the exocrine glands in estrogen-deficient mice may contribute to the development of autoimmune exocrinopathy, the molecular mechanism responsible for tissue-specific apoptosis remains obscure. Here we show that RbAp48 overexpression induces p53-mediated apoptosis in the exocrine glands caused by estrogen deficiency. RbAp48-inducible transfectant results in rapid apoptosis with p53 phosphorylation (Ser9) and α-fodrin cleavage. Reducing the expression of RbAp48 through small interfering RNA inhibits the apoptosis. Prominent RbAp48 expression with apoptosis was observed in the exocrine glands of C57BL/6 ovariectomized (OVX) mice but not in OVX estrogen receptor $\alpha^{-/-}$, $p53^{-/-}$, and $E2F\text{-}1^{-/-}$ mice. Indeed, transgenic expression of the RbAp48 gene induced apoptosis in the exocrine glands but not in other organs. These findings indicate that estrogen deficiency initiates p53-mediated apoptosis in the exocrine gland cells through RbAp48 overexpression and exerts a possible gender-based risk of autoimmune exocrinopathy in postmenopausal women.

Estrogenic action has been suggested to be responsible for the strong female preponderance of many autoimmune diseases, including systemic lupus erythematosus, rheumatoid arthritis, and Sjögren's syndrome (50, 51). Recent evidence suggests that apoptosis plays a key role in the physiology and pathogenesis of various autoimmune diseases (2, 7, 19, 35, 42). We have demonstrated that estrogenic action influences target epithelial cells through Fas-mediated apoptosis in a murine model for Sjögren's syndrome (13). Recently, we found that tissue-specific apoptosis in the exocrine glands spontaneously occurring in estrogen-deficient mice may contribute to the development of autoimmune exocrinopathy (14). We speculate that antiestrogenic actions might be a potent factor in the formation of pathogenic autoantigens. It has been reported that the antiestrogen tamoxifen (TAM) induces cell death in the human breast cancer cell line MCF-7 (17). We observed a time- and concentration-dependent increase in apoptosis of mouse and human salivary gland cells ([MSG] mouse primary culture; [HSG] human cell line) treated with TAM but not in other cell lines (HT-29, Colo201, and Jurkat) (14).

Apoptosis can be initiated by many different factors, but activation of caspases, which are a special class of proteolytic enzymes, is always involved in this process. Activation of caspases may be achieved by several molecular pathways; the best known stimuli triggering the caspase cascade are stimulation of Fas or TNF receptors, release of cytochrome *c* from the cellular mitochondria, and exposure to granzymes, which are secreted by cytotoxic T cells (3, 12, 31, 37, 54). Detailed research on the mechanisms controlling caspase activity will provide better insight into the pathogenesis of autoimmune diseases with special reference to estrogen deficiency. In this study, we have focused on the molecular mechanisms responsible for tissue-specific apoptosis caused by estrogen deficiency and identified RbAp48 as a novel apoptosis-inducing gene exclusively in the exocrine glands. Retinoblastoma (Rb) protein is a multifunctional protein that binds to transcription factors and kinases to regulate both cell growth and apoptosis (11). Although recent data suggest that loss of Rb can cause apoptosis through derepression of basally inhibited extrinsic apoptotic pathway genes (20), no mechanism has provided a molecular explanation for RbAp48 in the induction of apoptosis.

* Corresponding author. Mailing address: Department of Oral Molecular Pathology, Institute of Health Biosciences, The University of Tokushima Graduate School, 3 Kuramotocho, Tokushima 770-8504, Japan. Phone: 81 88 633 7327. Fax: 81 88 633 7327. E-mail: hayashi@dent.tokushima-u.ac.jp.

MATERIALS AND METHODS

Cell culture and gene transfection. HSG, MSG, HT29, Colo201, HeLa, HepG2, SH-SY5Y, NEC14, THP-1, Jurkat, Raji, U937, and W138 cells were cultured in Dulbecco's modified Eagle medium (DMEM) or RPMI 1640 medium containing 10% fetal bovine serum at 37°C. HSG and MSG cells have been described elsewhere (38, 40). The following were used for cell cultures: 10^{-7} M TAM (Wako Pure Chemical, Osaka, Japan), 10^{-9} M β-2-estradiaol (E2; Wako), 10^{-7} M staurosporin (Wako), paclitaxel (Wako), 1 μM etoposide (Wako), 1 μM ICI182780 (Wako), 25 ng/ml anti-Fas monoclonal antibody (MAb) (MBL, Nagoya, Japan), and 10 ng/ml recombinant human gamma interferon (R&D Systems, Minneapolis, MN). The RbAp48 gene inserted into the pCMV (2N3T) vector, a gift from D. Trouche, was transfected into the cells using FuGENE6 Transfection Reagent (Roche Diagnostics Corp., Indianapolis, IN). The RbAp48-stable cell line (RH0) from HSG cells in which RbAp48 expression was regulated by isopropyl-1-thio-β-D-galactopyranoside (IPTG), was established using a LacSwitch II Inducible Mammalian Expression System (Stratagene, La Jolla, CA). Briefly, the repressor vector (pCMVLacI) and RbAp48-inserted operator vector (pOPRVI/MCS) were cotransfected into HSG cells with FuGENE6, and the RbAp48 expression of hygromycin and G418-resistant transfectants was controlled by IPTG. For infection of adenovirus vector, RbAp48 gene-transfected MSG cells from $p53^{-/-}$ or wild-type mice were infected with 100 multiplicities of infection of adenovirus vector including the p53 gene obtained from Toren Finkel (National Institutes of Health). MSG and mouse mammary glands (MMG) were removed, placed in DMEM containing 10% fetal calf serum (FCS) and 10 mM HEPES (pH 7.4), and rapidly minced. The mate-

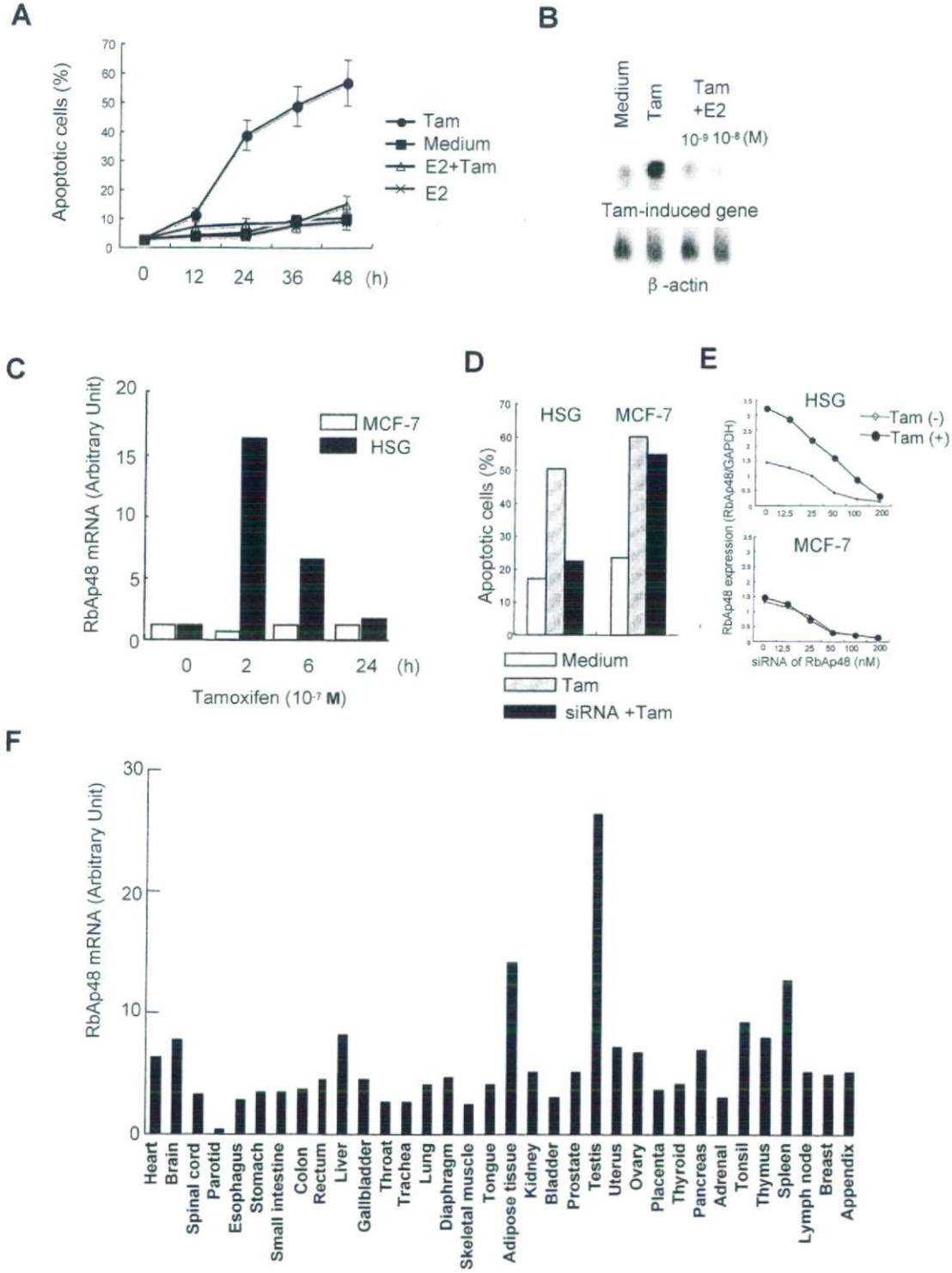

FIG. 1. Identification of the RbAp48 gene in salivary gland cell apoptosis. (A) A time-dependent increase in apoptotic HSG cells stimulated with TAM (10^{-7} M) was observed, and E2 (10^{-9} M) treatment inhibited apoptosis. Apoptotic cells were detected by flow cytometry using FITC-conjugated annexin V. (B) TAM-induced gene fragments cloned by differential display PCR were used as a probe by Northern blotting with mRNA from HSG cells treated with TAM (10^{-7} M) or E2 (10^{-9}M and 10^{-8}M). β-Actin mRNA was detected as an internal control. Each blot is representative of three independent experiments. (C) Analysis of RbAp48 mRNA expression was performed using total RNA from TAM-stimulated HSG and MCF-7 cells for 0 to 24 h. The graph is representative of three independent experiments. (D) The inhibitory effects of siRNA on TAM-induced apoptosis in HSG cells with siRNA (15 nM) of the RbAp48 construct but not in MCF-7 cells. After transfection of siRNA of RbAp48 and a fluorescence-labeled control gene, the cells were incubated with TAM (10^{-7} M) for an additional 24 h. Apoptosis was estimated by flow cytometric analysis using PE-conjugated annexin V. The graph is representative of three independent experiments. (E) A dose-dependent inhibition of siRNA (0 to 200 nM) of TAM-induced RbAp48 expression in HSG cells, not MCF-7 cells, was observed. The graph is representative of two independent experiments. (F) RbAp48 mRNA expression levels were analyzed using human tissue total RNA-blotted membrane. Message levels (arbitrary units) were quantified by BAS-2000II and expressed as the ratio of RbAp48 mRNA/β-actin mRNA. The graph is representative of two independent experiments.

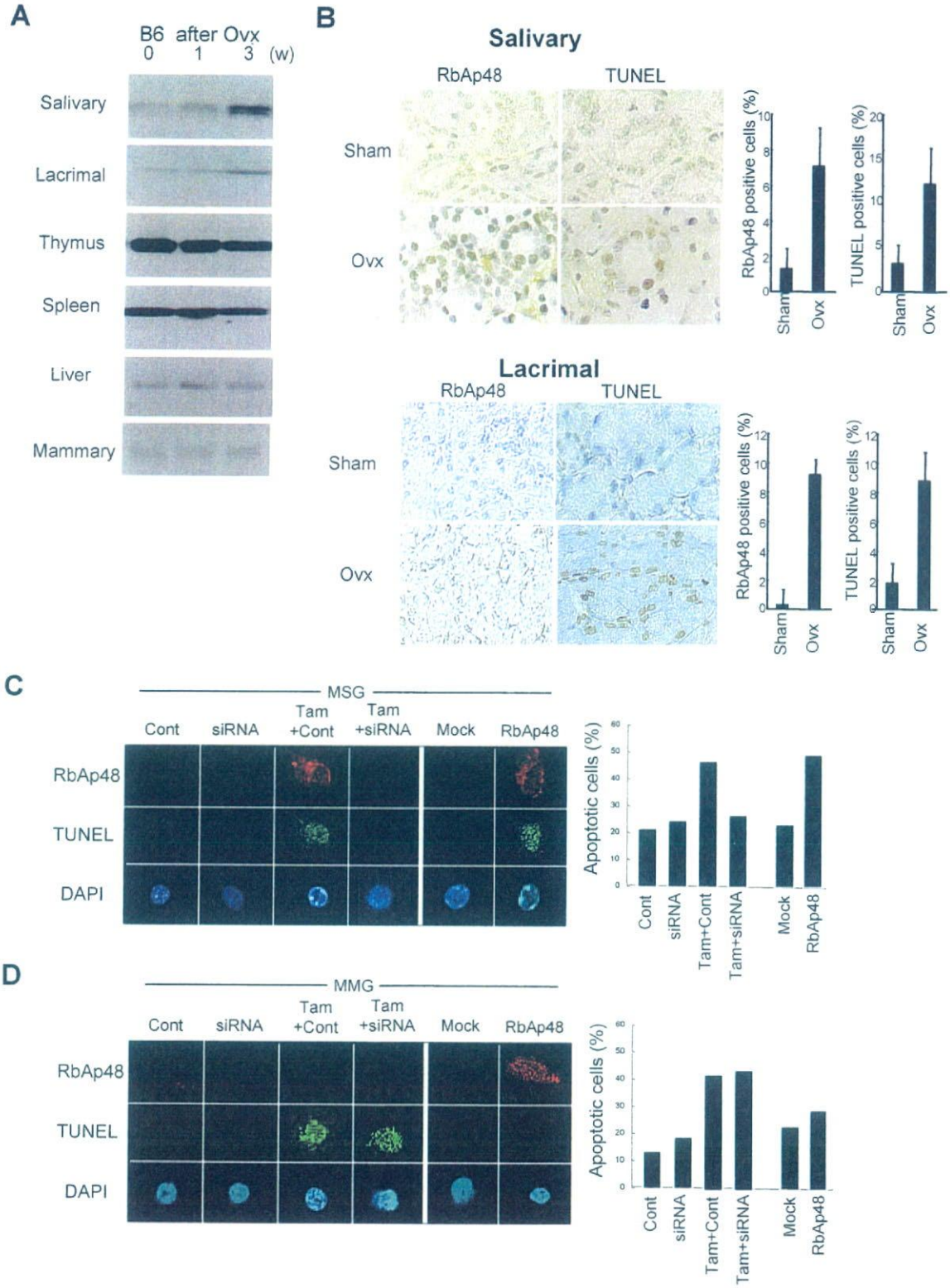

FIG. 2. RbAp48 overexpression in OVX B6 mice. (A) Increased RbAp48 expression in salivary and lacrimal gland tissues in OVX B6 mice from 0 to 3 weeks (age of mice, 4 to 7 weeks). Expression levels of RbAp48 in thymus, spleen, liver, and mammary glands from OVX B6 mice were constant. Western blot analysis was performed on proteins from tissue homogenates of OVX and sham mice. Blots were representative of three independent experiments. (B) Detection of $RbAp48^+$ and $TUNEL^+$ cells in salivary and lacrimal glands from OVX B6 and sham B6 mice at the age of 7 weeks. Immunohistochemical analysis of RbAp48 and in situ TUNEL assays were performed on the sections of salivary and lacrimal glands from OVX and sham mice. Images are representative of sections from five mice. The percentage of $RbAp48^+$ and $TUNEL^+$ cells in salivary and lacrimal glands was enumerated using a 10- by 20-mm grid covering an objective area of 0.16 mm^2. Data were analyzed in 10 fields per section and expressed as mean percent ± standard deviation of data from five mice. (C) TAM-induced apoptosis was associated with RbAp48 expression in

rials were then digested for 1 h at 37°C with 750 U/ml collagenase (Wako), 500 U/ml hyarulonidase type IV (Sigma), 1% bovine serum albumin, and 10 mM HEPES (pH 7.4) in DMEM. After digestion, they were filtered through a 70-μm nylon mesh, centrifuged, and rinsed twice with DMEM containing 10% FCS. These cells were cultured in chamber slides (Nalge Nunc International, Denmark) at a density of 5×10^4/well with DMEM containing 10% FCS. After cells were cultured for 24 h, the medium was changed to HuMedia-KG2 (Kurabo, Osaka, Japan).

Differential display analysis and Northern blotting. Total RNA was isolated from TAM-treated or nontreated HSG cells and reverse transcribed for differential display PCR with an RNAimage kit (Gene Hunter, Nashville, TN). TAM-induced cDNA fragments were gel excised and subcloned for TA vector. The clones were screened with a cDNA library derived from mRNA of TAM-stimulated HSG cells. The screened clone was transformed to plasmid and sequenced. Expressions of RbAp48 mRNA were detected by Northern blot analysis using ^{32}P-labeled RbAp48 cDNA probe. Equal loading of the gel was confirmed by using β-actin cDNA probe. In addition, the human total RNA-blotted membrane (Biocain Institute, Inc., San Leandro, CA) was used for analysis of RbAp48 mRNA in various human tissues.

Apoptosis detection assay. Apoptosis was detected using the annexin V-fluorescein isothiocyanate (FITC) apoptosis detection kit (Genzyme Corp., Cambridge, MA). Briefly, after cultured cells were washed with phosphate-buffered saline, the cells were incubated with FITC-conjugated annexin V and propidium iodide (PI) for 10 min at room temperature in the dark. Binding buffer was added, and apoptotic cells were detected by flow cytometric analysis with an EPICS flow cytometer (Beckman Coulter, Inc., Miami, FL).

Mice. Estrogen receptor α-deficient ($ER\alpha^{-/-}$), $p53^{-/-}$, $E2F\text{-}1^{-/-}$, or C57BL/6 (B6) mice were purchased from Taconic (Germantown, NY), Jackson Laboratory (Bar Harbor, ME), or Nihon Clea (Tokyo, Japan). These mice were subjected to ovariectomy (OVX mice) and or to a sham operation (sham mice) at 4 weeks of age. At 0 to 3 weeks after OVX, all organs were evaluated by pathological or immunohistochemical analysis. To generate the RbAp48-transgenic (TG) mice, B6 mice were used to obtain fertilized eggs, and the gene fragment containing RbAp48 cDNA regulated by salivary gland-specific promoter (22) (provided by B. B. Larsen) was microinjected into the pronucleus of fertilized eggs to establish the transgenic lines. Histopathological analysis of all organs of RbAp48-TG mice screened by PCR was performed. All mice were maintained in our specific-pathogen-free facility.

siRNA of RbAp48. Small interfering RNA (siRNA) corresponding to the coding sequence +136 to +156 of the RbAp48 gene was synthesized by Hokkaido System Science (Sapporo, Japan) according to standard methods (23, 52) for the following: sense, CGAGGAAUACAAAAUAUGGTT; antisense, CCA UAUUUUGUAUUCCUCGTT. siRNA of the glyceraldehyde-3-phosphate dehydrogenase (GAPDH) gene (Ambion, Austin, TX) was used as a control. siRNA (0 to 50 nM) and 1 μg of pCMV-green fluorescent protein (GFP) plasmid were cotransfected into HSG, MCF-7 cells, and the IPTG-controlled RbAp48-stable cell line (RH0) using a Silencer siRNA Transfection II Kit (Ambion) or FuGENE6 (Roche). At 24 h after cotransfection, RH0 cells were incubated with IPTG for an additional 24 h. GFP^+ apoptotic cells were detected by flow cytometry using phycoerythrin (PE)-conjugated annexin V.

E2F-1, ARF, and p53 siRNA. For siRNA of E2F-1, ARF, and p53, an siTrio Full Set (B-Brigde International, Sunnyvale, CA) was used for HSG cells. Briefly, each cocktail including the three RNA oligonucleotides listed below was transfected into cells with a Quick-Step Transfection Kit (B-Brigde International). Sequences of the oligonucleotide sets are as follows: for E2F-1, CCAACGUCCU UGAGGGCAUTT (sense), AUGCCCUCAAGGACGUUGGTT (antisense), CU GCAGAGCAGAUGGUUAUTT (sense), AUAACCAUCUGCUCUGCAGTT (antisense), GGAAAGUGAGGGAGGGAGATT (sense), and UCUCCCUCCC UCACUUUCCTT (antisense); for ARF, GCUCACCUCUGGUGCCAAATT (sense), UCACCAAGAACCUGCGCACTT (antisense), GGGUUUUCGCGGU UCACAUTT (sense), AUGUGAACCACGAAAACCCTT (antisense), GGGUU UUCGUGGUUCACAUTT (sense), and AUGUGAACCACCACGAAAAC CCTT (antisense), for p53, GGAAACUACUUCCUGAAAATT (sense), UUUU CAGGAAGUAGUUUCCTT (antisense), CUGGAAGACUCCAGUGGUATT (sense), UACCACUGGAGUCUUCCAGTT (antisense), CUUAGUACCUAAA AGGAAATT (sense), and UUUCCUUUUAGGUACUAAGTT (antisense). Transfected cells were incubated with or without TAM, and confocal or flow cytometric analysis was performed.

Western blotting. Whole-cell extracts of HSG or RH0 cells were purified using radioimmunoprecipitation assay buffer (50 mM Tris-HCl, pH 7.4, 150 mM NaCl, 1 mM EDTA, 1% NP-40, 1 mM dithiothreitol [DTT], 1 mM phenylmethylsulfonyl fluoride) supplemented with a protease inhibitor cocktail (Sigma Chemical Co., St. Louis, MO). After centrifugation for 20 min at 12,000 rpm at 4°C, the supernatant was extracted and used for samples. Also, to detect α-fodrin in organs, tissue samples from OVX and sham C57BL/6 mice were extracted as described above. Ten micrograms of each sample per well was used for 7.5 to 12.5% sodium dodecyl sulfate-polyacrylamide gel electrophoresis and transferred to polyvinylidene difluoride membranes, which were probed with anti-RbAp48, anti-Rb (p110 and p130), anti-Bad, anti-Bax, anti-ARF (p14 and p19), anti-cyclin D3 (BD Transduction Laboratories, Lexington, KY), anti-Mdm2, anti-E2F-1, anti-phospho-Rb (Sigma), anti-p53, anti-phospho-p53 Ab sampler kit (Ser6, Ser9, Ser15, Ser20, Ser37, Ser46, and Ser392; Cell Signaling Technology Inc., Beverly, MA), anti-α-fodrin (Affiniti, Mamhead, United Kingdom), and anti-p21 (Santa Cruz Biotechnology, Santa Cruz, CA) as the primary Abs, and anti-α-tubulin, GAPDH, or histone MAb (Sigma) as internal control. The nitrocellulose membranes were incubated with peroxidase-conjugated horse anti-mouse or rabbit immunoglobulin G (IgG; Vector Laboratories) as the secondary Ab. Protein binding was visualized with ECL Western blotting reagent (Amersham Corp., Arlington Heights, IL).

TUNEL assay. Apoptotic cells were detected in sections using the in situ terminal deoxynucleotidyltransferase (TdT)-mediated dUTP-biotin nick end labeling (TUNEL) kit (Wako). Sections were incubated with proteinase K (20 μg/ml) for 10 min and then presoaked in TdT buffer (0.5 μM cacodylate, 1 mM CoCl, 0.5 μM DTT, 0.05% bovine serum albumin, 0.15 M NaCl) for 10 min. Sections were incubated for 2 h at 37°C in 25 μl of TdT solution, containing 1× terminal transferase buffer, 0.5 nmol of biotin-dUTP, and 10 U of TdT. After the TdT reaction, sections were soaked in TdT blocking buffer (300 nM NaCl, 30 mM Tris-sodium citrate-2-hydrate), incubated with horseradish peroxidase-conjugated streptavidin for 30 min at room temperature, and developed for 10 min in phosphate-buffered citrate (pH 5.8) containing 0.6 mg/ml DAB (3,3′-diaminobenzidine-tetrahydrochloride-dihydrate). Nuclei were counterstained with hematoxylin. For confocal microscopic analysis, FITC-labeled UTP was used.

Caspase activity assay. Caspase activities were assayed using a caspase family colorimetric substrate set (BioVision Inc.). Briefly, 100 μg of cytoplasmic lysates of RH0 cells was incubated with 200 μM Ac-YVAD-pNA (caspase 1 substrate), Ac-VDVAD-pNA (caspase 2 substrate), Ac-DEVD-pNA (caspase 3 substrate), Ac-WEHD-pNA (caspase 5 substrate), Ac-VEID-pNA (caspase 6 substrate), Ac-IETD-pNA (caspase 8 substrate), and Ac-LEHD-pNA (caspase 9 substrate) at 37°C for 1 h. The absorbance of samples was read at 405 nm in a microtiter plate reader. The relative percent increase in caspase activity was determined by comparing these results with the level of the uninduced control.

Gel shift assay. Nuclear extracts were prepared from RH0 cells by a method previously described (29). Nuclear extracts containing 5 μg of protein were incubated in 20 μl of binding buffer (10 mM Tris-HCl, pH 8.0, 50 mM NaCl, 1 mM MgCl2, 0.5 mM DTT, and 4% glycerol) with or without a cold competitor. The E2F-1 DNA probe, 5′-TCCGTAGTTTTCGCGCTTAAATTTGAGAAAG GGCGCGAAACTAGTC-3′ (10,000 cpm) labeled with [γ-^{32}P]ATP was added, and the samples were incubated at room temperature for 20 min. Reaction mixtures were separated in a 4% polyacrylamide gel and autoradiographed on X-ray film (Fujifilm, Kanagawa, Japan).

Immunohistochemical analysis. Immunohistochemical analysis of RbAp48 expression was performed on the sections of salivary and lacrimal glands from sham, OVX B6, RbAp48-WT (wild type), and RbAp48-TG mice. Paraffin-embedded sections were stained with anti-RbAp48 MAb (BD Transduction Laboratories) as the primary Ab. Protein binding was detected with an LSAB2 kit containing horseradish peroxidase (DAKO, Carpineteria, CA) and DAB as a substrate. The counterstaining of nuclei was performed with hematoxylin.

Confocal microscopy. Confocal microscopic analysis of RbAp48, E2F-1, ARF, and p53 expression, and TUNEL-positive cells was performed on the cultured cells, and frozen sections of salivary glands from sham, OVX $ER\alpha^{-/-}$, $p53^{-/-}$,

MSG cells from B6 mice, and the inhibitory effects with siRNA of RbAp48 construct were observed by confocal microscopic analysis. The percentage of $TUNEL^+$ apoptotic cells was enumerated as described. Cont, irrelevant siRNA control. Images are representative of three independent experiments. (D) TAM-induced apoptosis was not associated with RbAp48 expression in the primary culture of MMG cells from B6 mice. $TUNEL^+$ apoptotic cells were enumerated as described. Images are representative of three independent experiments.

$E2F1^{-/-}$, RbAp48-WT, and RbAp48-TG mice using a Confocal Laser Microscan (LSM 5 PASCAL; Carl Zeiss, Germany). As the second Abs, Alexa Fluor 488–anti-mouse IgG heavy and light chain [IgG (H+L)], Alexa Fluor 568–goat anti-rabbit IgG (H+L), Alexa Fluor 488–donkey anti-rat IgG (H+L), Alexa Fluor 488–chicken anti-goat IgG (H+L), and Alexa Fluor 568–rabbit anti-goat IgG (H+L) were used. Nuclear DNA was stained with 4′,6-diamidino-2-phenylindole dihydrochloride.

BrdU incorporation. MSG cells from RBAp48 TG and WT mice were stimulated with phorbol 12-myristate 13-acetate for 24 h, and 10 mM bromodeoxyuridine (BrdU) was incorporated for the last 2 h. Fixed and permeabilized cells were treated with DNase and stained with FITC-conjugated anti-BrdU antibody (BD Pharmingen, San Diego, CA). The polyvinylidene difluoride DNA synthetic activity was analyzed by flow cytometry.

RESULTS

Identification of TAM-induced gene. We found a time-dependent increase in apoptotic HSG cells stimulated with TAM, and E2 treatment inhibited the apoptosis (Fig. 1A). To identify gene products specific to TAM-induced apoptosis in the salivary gland cells, mRNAs from HSG cells treated with TAM and nontreated cells were analyzed by a differential display PCR method. From the samples isolated with the highest grade of differential expression, we analyzed the mRNAs from HSG cells treated with TAM and nontreated cells by a reverse Northern blotting technique (Fig. 1B). The sequence of TAM-induced mRNA corresponds (100%) to RbAp48. The expression of RbAp48 mRNA in HSG cells reached peak level at 2 h after stimulation with TAM, and then the level decreased, whereas increased expression of RbAp48 mRNA in MCF-7 cells was not observed (Fig. 1C). We confirmed the inhibitory effects of siRNA on TAM-induced apoptosis in HSG cells, not MCF-7 cells, with siRNA (5 to 50 nM) of RbAp48 construct (Fig. 1D). In addition, a dose-dependent inhibition of siRNA (0 to 200 nM) on TAM-induced RbAp48 expression in HSG cells, not MCF-7 cells, was observed (Fig. 1E). We next searched the tissue distribution of RbAp48 mRNA using human tissue total RNA-blotted membrane by Northern blot analysis. We found the highest level of expression of RbAp48 mRNA in the testis, which is consistent with the previous report (33), and the lowest was found in the parotid salivary gland (Fig. 1F), although the molecular mechanism by which the lowest RbAp48 mRNA is expressed in the parotid glands is unclear.

RbAp48 overexpression in estrogen-deficient mice. To confirm the in vivo overexpression of RbAp48 and apoptosis in estrogen-deficient B6 mice, OVX was performed on mice at the age of 4 weeks. Using Western blotting, we detected a time-dependent increase in RbAp48 in the salivary and lacrimal gland tissues from 0 to 3 weeks after OVX (at the age of 4 to 7 weeks) but not in other organs, including mammary glands (Fig. 2A). $RbAp48^+$ and $TUNEL^+$ apoptotic cells were detected by immunohistochemical analysis in the salivary and lacrimal gland sections from OVX B6 mice at the age of 7 weeks but not in sham mice (Fig. 2B). In vitro studies using primary cultured cells from B6 mice demonstrated that TAM-induced apoptosis was associated with RbAp48 expression in MSG cells but not in MMG cells (Fig. 2C and D). We confirmed the inhibitory effects of siRNA in MSG cells but not in MMG cells with siRNA of RbAp48 construct (Fig. 2C and D).

RbAp48 as a novel apoptosis-inducible gene. RbAp48 mRNA expression and apoptosis could be induced in HSG cells stimulated with TAM and a pure antiestrogen, ICI182780, but not with other apoptotic stimuli such as staurosporin, paclitaxel, anti-Fas MAb, and etoposide (Fig. 3A). This indicates that induction of RbAp48 mRNA expression might be dependent on estrogen deficiency. To ensure the role of RbAp48 in various types of cells, RbAp48 was transiently transfected, and apoptosis was determined by flow cytometry using an annexin V-FITC apoptosis detection kit. Among the cells examined (HSG, MSG, MCF-7, HT-29, Colo201, HeLa, HepG2, SH-SY5Y, NEC14, THP-1, Jurkat, Raji, U937, and WI38), significant apoptosis was induced exclusively in the salivary gland cells transfected with RbAp48 of both human and mouse origin (Fig. 3B). Notably, apoptosis was induced by transfection with RbAp48 cDNA in MSG cells isolated from $ER\alpha^{-/-}$ mice, indicating that this signaling might act in the downstream of estrogen-ER binding. Apoptotic cells could not be induced by the transgene of RbAp48 cDNA but was induced by TAM in MCF-7 cells. We confirmed that the induction levels of RbAp48 are the same in the other cell lines including Jurkat and THP-1 as the HSG cells (Fig. 3C). We next generated and analyzed the RbAp48-stable cell line (RH0), which was an IPTG-inducible transfectant of RbAp48 in HSG cells, with a LacSwitch II Inducible Mammalian Expression System using repressor and operator vectors. Apoptosis was drastically induced in IPTG-treated RH0 cells in association with RbAp48 expression within 8 h (Fig. 3D). When we examined the effect of siRNA on RbAp48-induced apoptosis, the apoptosis in IPTG-treated RH0 cells was clearly inhibited by siRNA of RbAp48 but not by siRNA of GAPDH or an irrelevant control (Fig. 3E).

Molecular mechanisms for RbAp48-induced apoptosis. We next examined the molecular mechanisms responsible for RbAp48-induced apoptosis. We detected upregulation of phosphorylated Rb, cyclin D3, p14ARF, Bax, Bad, cytochrome *c* (Cyt *c*) and a cleavage product of α-fodrin (arrow) in IPTG-treated RH0 cells (Fig. 4A). Our previous report demonstrated that α-fodrin is a candidate autoantigen of primary Sjögren's syndrome (10). When nuclear extracts of IPTG-treated RH0 cells were analyzed by gel shift assay, DNA binding activity of E2F-1 was detected in RbAp48-induced apoptotic cells (Fig. 4B). E2F-1 protein was also detected in the nuclear extract by Western blotting (Fig. 4B). It has been proposed that the E2F-1 transcription factor serves as a link between the Rb/E2F proliferation pathway and the p53 apoptosis pathway by inducing the expression of p14ARF, a protein that regulates p53 stability (36). We next focused on the p53-dependent pathway, because MSG cells transfected with RbAp48 isolated from $p53^{-/-}$ mice are apoptosis resistant (Fig. 4C). When Adp53-infected MSG cells were transfected with the RbAp48 gene, apoptosis was rapidly induced (Fig. 4C). Phosphorylated p53 (Ser9) was found by Western blotting after 2 to 4 h, but no other phosphorylated p53 (Ser15, Ser20, and Ser392) was detected (Fig. 4D). The phosphorylation of p53 in the other sites (Ser6, Ser37, and Ser46) was not observed (data not shown). We also confirmed a time-dependent downregulation of Mdm2 (Fig. 4D), which is important as a regulatory partner of p53 (47). Using Western blotting, we also detected increased p21 expression, a major player in the p53-mediated pathway, in IPTG-treated RH0 cells (Fig. 4E). p53 induces apoptosis by a multitude of molecular pathways, in addition to transactivation

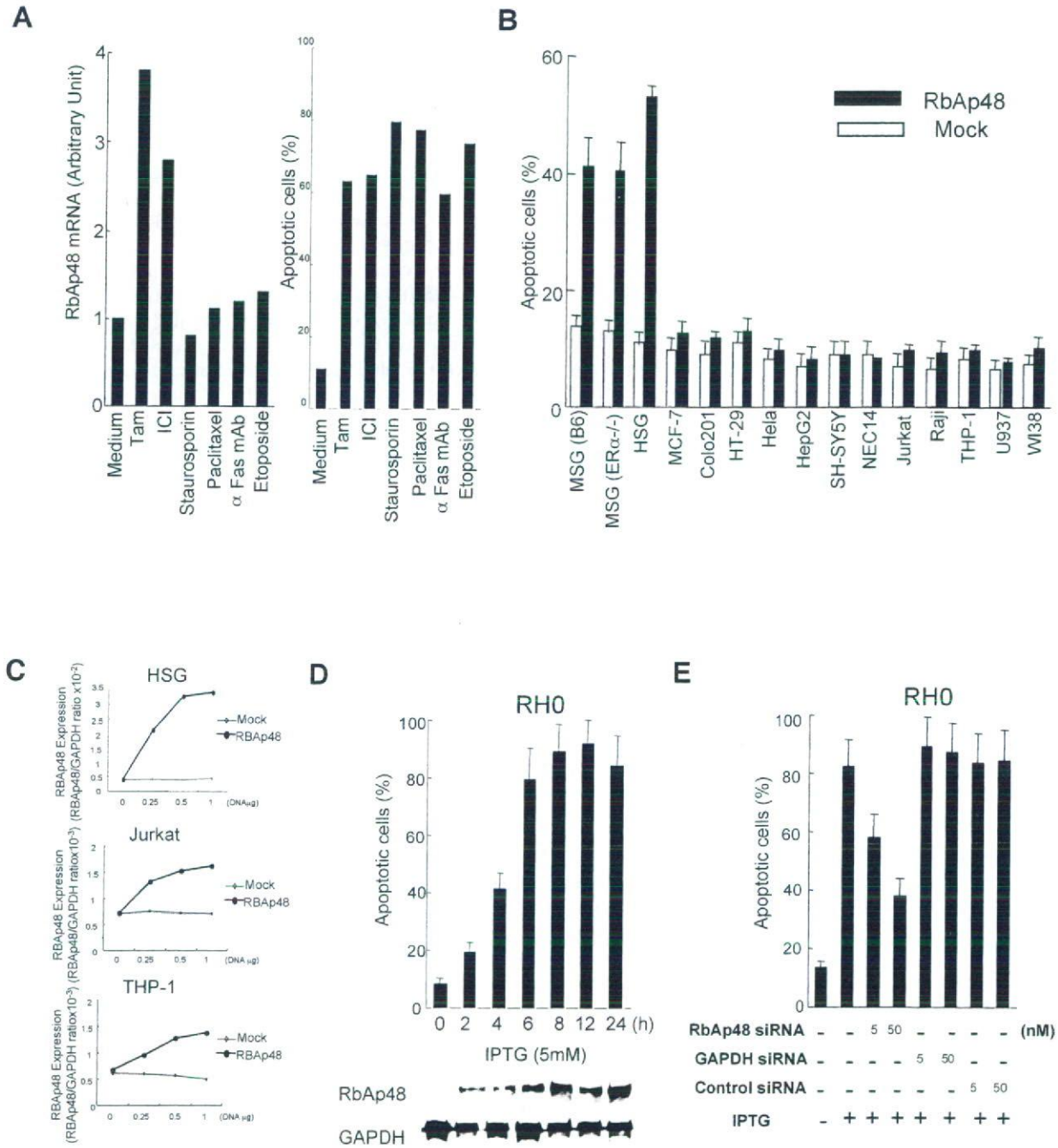

FIG. 3. Role of RbAp48 in salivary gland cell apoptosis. (A) HSG cells were treated with antiestrogenic reagents (10^{-7} M TAM and 10^{-7} M ICI182780) and general apoptotic stimuli (staurosporin, paclitaxel, anti-Fas MAb, and etoposide). RbAp48 mRNA was quantitated with BAS-2000II, and message level was expressed as the ratio of RbAp48 mRNA/β-actin mRNA; the percentage of apoptotic cells was detected by FITC-annexin V-PI was expressed for all of these agents. Graphs are representative of three independent experiments. (B) The RbAp48 gene was transiently transfected into various cells using FuGENE6. At 48 h after transfection of pCMV-RbAp48 plasmid or pCMV (mock) plasmid, apoptotic cells were detected by FITC-annexin V-PI. Data are the means ± standard deviations of triplicate samples. The graph is representative of three independent experiments. (C) The levels of the induction ratio of RbAp48 were shown to be the same in the other cell lines including Jurkat and THP-1 as the HSG cells using Western blot analysis. The levels were expressed as the ratio of RbAp48/GAPDH protein. (D) Establishment of the RbAp48 stable cell clone. An increase in RbAp48 expression and apoptosis of IPTG-treated RH0 cells were observed in a time-dependent manner. Apoptotic cells were detected by FITC-annexin V-PI. Data are means ± standard deviations of triplicate samples. Expressions of RbAp48 and GAPDH as an internal control were detected by Western blot analysis. Graph and images are representative of four independent experiments. (E) Inhibitory effects of siRNA on RbAp48-induced apoptosis. IPTG-treated RH0 cells were cotransfected with siRNA (5 to 50 nM) of RbAp48 and pCMV-GFP. Apoptotic cells gated on GFP^+ were detected by PE-conjugated annexin V. Data are means ± standard deviations of triplicate samples. Graph is representative of three independent experiments.

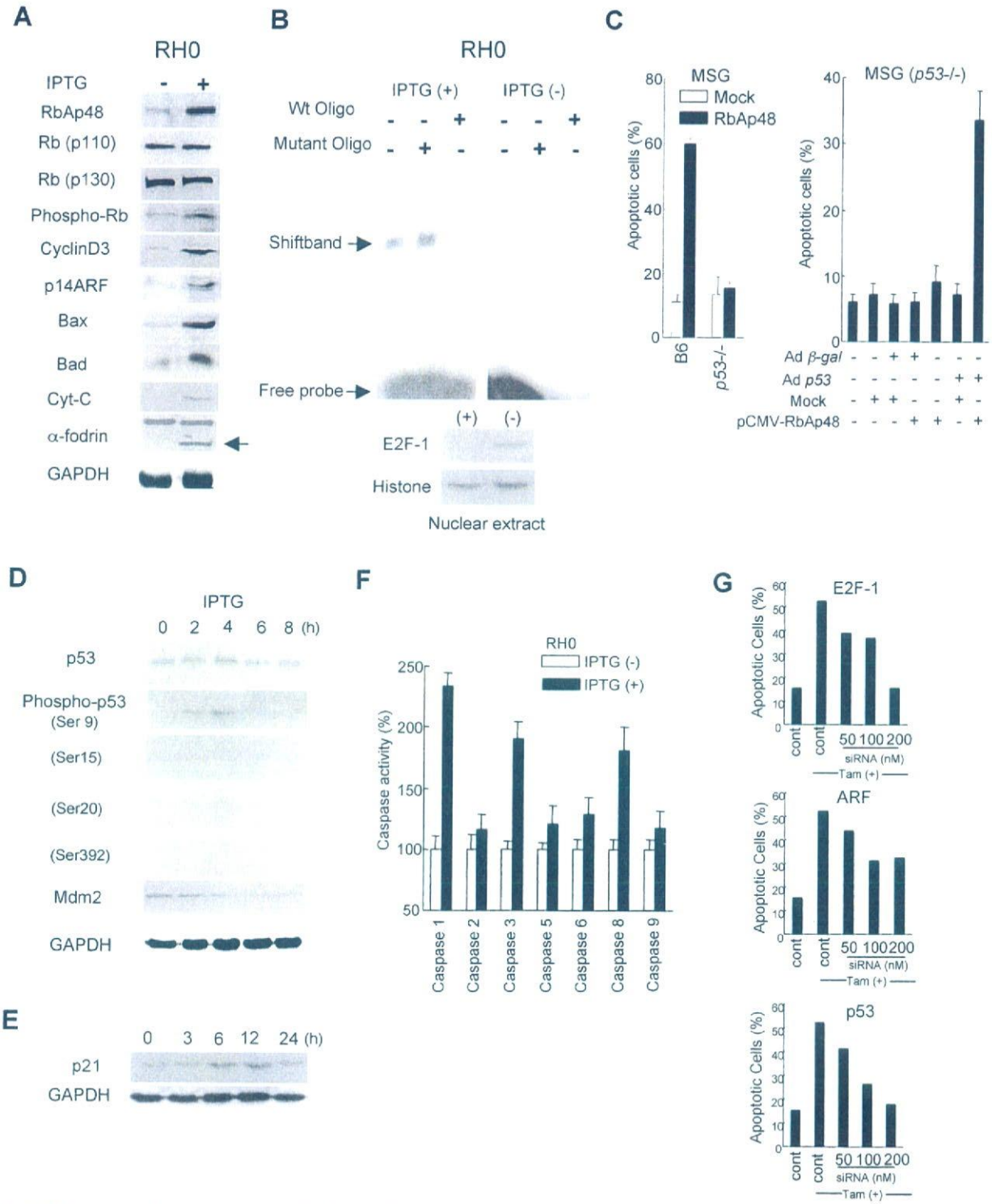

FIG. 4. Molecular mechanisms responsible for RbAp48-induced apoptosis. (A) Contribution of cell cycle and mitochondrion-related molecules in RbAp48-induced apoptosis of RH0 cells. The lysates of IPTG-treated or nontreated RH0 cells were used to detect RbAp48, Rb (p110 and p130), phospho-Rb, cyclin D3, p14ARF, Bax, Bad, Cyt-*c*, the cleavage product of α-fodrin, and GAPDH for Western blot analysis. Blots are representative of three independent experiments. (B) Detection of E2F-1 transcriptional activity in RbAp48-induced apoptosis. The nuclear proteins of IPTG-treated RH0 cells were analyzed by gel shift assay with an E2F-1 binding DNA probe. To confirm the specific binding to the E2F-1 binding site, the mutant oligonucleotide and wild-type oligonucleotide as a competitor were used for this assay. E2F-1 protein was detected in the nuclear extract by Western blotting. Histone was used for an internal control. Blots are representative of three independent experiments. (C) Apoptosis of MSG cells from $p53^{-/-}$ mice was not observed by RbAp48 gene transfection. Transfection with pCMV (Mock) was used as control. MSG ($p53^{-/-}$) cells were infected with Ad*p53* and incubated for 24 h. The infected cells were cotransfected with the RbAp48 gene and

of target genes, and it can elicit apoptosis by transcription-independent mechanisms (5, 28). Although apoptosis in response to p53 activation is often accompanied by caspase activation, the mechanisms underlying p53-induced caspase activation remain poorly understood. Caspase activities in RbAp48-induced apoptosis in HSG cells were assayed using a caspase family colorimetric substrate set. A significant increase in caspase 1 activity was detected with relatively elevated caspase 3 and 8 activity on RbAp48-induced apoptotic HSG cells (Fig. 4F). RbAp48-induced apoptosis in HSG cells was clearly inhibited by siRNA of E2F-1 and p53 but only moderately by siRNA of ARF (Fig. 4G).

RbAp48/E2F1/ARF-p53 pathway in the salivary glands. We evaluated the effects of RbAp48 overexpression and knockdown in primary MSG cells and documented the effects on E2F-1, ARF, and p53 protein levels in these cells. We demonstrated that overexpression of RbAp48 in MSG cells from B6 mice induced E2F-1, p19ARF, and phospho-p53 expression, and the inhibitory effect of siRNA of RbAp48 was observed from confocal microscopic analysis (Fig. 5A). We next examined whether TAM-induced apoptosis is associated with RbAp48 expression in MSG cells from B6 mice, compared with cells from $ER^{-/-}$, $E2F1^{-/-}$, and $p53^{-/-}$ mice. By confocal microscopic analysis, we found that TAM-induced apoptosis was associated with RbAp48 expression in MSG cells from B6 mice but not from $ER^{-/-}$, $E2F1^{-/-}$, and $p53^{-/-}$ mice Fig. (5B). We further examined the effect of OVX on the expression of RbAp48, E2F-1, p19ARF, and phospho-p53 in MSG cells from B6, $ER^{-/-}$, $E2F1^{-/-}$, and $p53^{-/-}$ mice. By double-labeled confocal microscopy, we found coexpression of RbAp48/E2F1, RbAp48/p19ARF, and RbAp48/p53 in MSG cells from OVX B6 mice but not from B6 mice (Fig. 5C). No differences in RbAp48/E2F1, RbAp48/p19ARF, and RbAp48/phospho-p53 expression levels were observed in MSG cells from non-OVX and OVX $ER^{-/-}$, $E2F1^{-/-}$, and $p53^{-/-}$ mice (Fig. 5C).

Findings in RbAp48-transgenic mice. We constructed several lines of B6 background TG mice (39) expressing RbAp48 in the salivary glands using Lama promoter as described in Materials and Methods. Prominent expression of RbAp48 in the salivary glands from TG mice was determined at the age of 8 to 20 weeks by both immunohistochemistry and Western blotting (Fig. 6A and B). No difference in RbAp48 expression in the spleen was observed between TG and WT mice. A considerable number of $TUNEL^+$ apoptotic epithelial duct cells were found in the salivary glands of RbAp48-TG mice but not WT mice at the age of 20 weeks (Fig. 6C). In addition, expression of E2F-1, p19ARF, and phospho-p53 was observed in the salivary glands of RbAp48-TG mice but not WT mice (Fig. 6D). BrdU studies of TG mice with ectopic RbAp48 in the salivary glands demonstrated that cellular proliferation is barely affected (Fig. 6E). No pathological findings were observed in other organs of TG mice.

DISCUSSION

In this study, we demonstrated the first evidence that gender-based, tissue-specific apoptosis could be induced in the exocrine gland cells through RbAp48 overexpression with p53 phosphorylation. Indeed, RbAp48 overexpression with apoptosis was observed in the exocrine glands in OVX C57BL/6 mice, and transgenic expression of the RbAp48 gene induced tissue-specific apoptosis in the exocrine glands.

RbAp48, initially identified as a retinoblastoma binding protein (34), was characterized as a component of distinct nucleosome-modifying complexes, including the nuclear histone deacetylases (18, 25). In general, the functions of the RbAp48-like proteins in these complexes remain undetermined. It was reported that E2F-1 and RbAp48 are physically associated in the presence of Rb and histone deacetylase (26), suggesting that RbAp48 could be involved in transcriptional repression of E2F-responsive genes. The induction of apoptosis in various cell lines is accompanied by a shift in Rb from the hyper- to the hypophosphorylated form (49). Rb dephosphorylation, which has been shown to be required for apoptosis, occurs in the early stage of apoptosis (6). Loss of Rb function can induce p53-dependent apoptosis, but little is known about the mechanisms of Rb-regulated p53-dependent apoptosis. Recently, Lieman et al. provided evidence for a novel mechanism linking Rb-E2F to the extrinsic apoptotic pathway through inactivation of focal adhesion kinase and activation of caspase 8 (20). It has been proposed that the E2F-1 transcription factor serves as a link between the Rb/E2F proliferation pathway and the p53 apoptosis pathway by inducing the expression of p14ARF, a protein that regulates p53 stability. Recent observations have revealed that p53 can directly translocate to mitochondria and induce apoptosis in a transactivation-independent manner (21). In this study, we confirmed a time-dependent downregulation of Mdm2, which is important as a regulatory partner of p53 (47). In addition to regulation of p53, Mdm2 has been reported to stimulate E2F-1 transactivation by a mechanism that remains unclear. E2F-1 can signal p53 phosphorylation in the absence of p14ARF, similar to the observed modifications to p53 in response to DNA damage. p53 modification is found to be crucial for E2F-1-mediated apoptosis, and this apoptosis is compromised when E2F-1 is coexpressed with a p53 mutant

pCMV-GFP, and then apoptosis was detected by PE-annexin V on GFP^+ cells. Infection of adenovirus β-galactosidase was used as a control. Graphs are representative of five independent experiments. (D) Expression levels of p53, phospho-p53 (Ser9), and Mdm2 in IPTG-treated RH0 cells. Other phosphorylated p53 proteins (Ser15, Ser20, and Ser392) were not detected. GAPDH expression was used for an internal control. Blots are representative of three independent experiments. (E) Detection of increased p21 expression, a major player in the p53-mediated pathway, by Western blotting. Blot is representative of two independent experiments. (F) Caspase activities of IPTG-treated RH0 cells were analyzed by a caspase enzymatic activity assay. A significant increase in caspase-1 activity was detected with relatively elevated caspase 3 and 8 activity. The absorbance of samples was read at 405 nm in a microtiter plate reader and the relative percent increase in activity was calculated by comparing the absorbance of IPTG-treated cells with that of untreated cells. Data are means ± standard deviations of triplicate samples. The graph is representative of three independent experiments. (G) RbAp48-induced apoptosis in HSG cells was clearly inhibited by siRNAs of E2F-1 and p53 but only moderately by siRNA of ARF. Graphs are representative of three independent experiments.

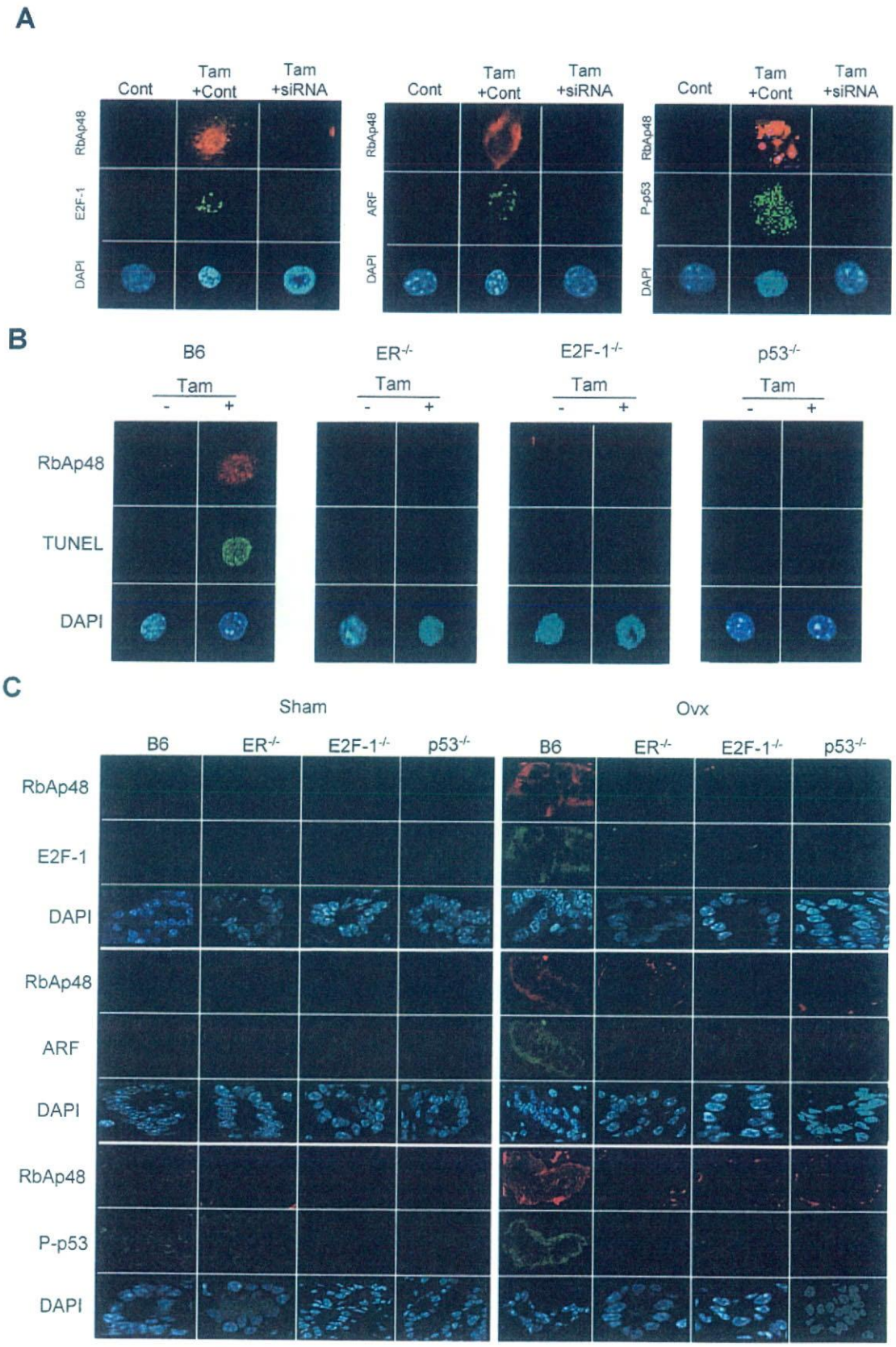
A
Cont
Tam +Cont
Tam +siRNA
RbAp48
E2F-1
DAPI
ARF
P-p53
B
B6
ER-/-
E2F-1-/-
p53-/-
Tam
TUNEL
C
Sham
Ovx

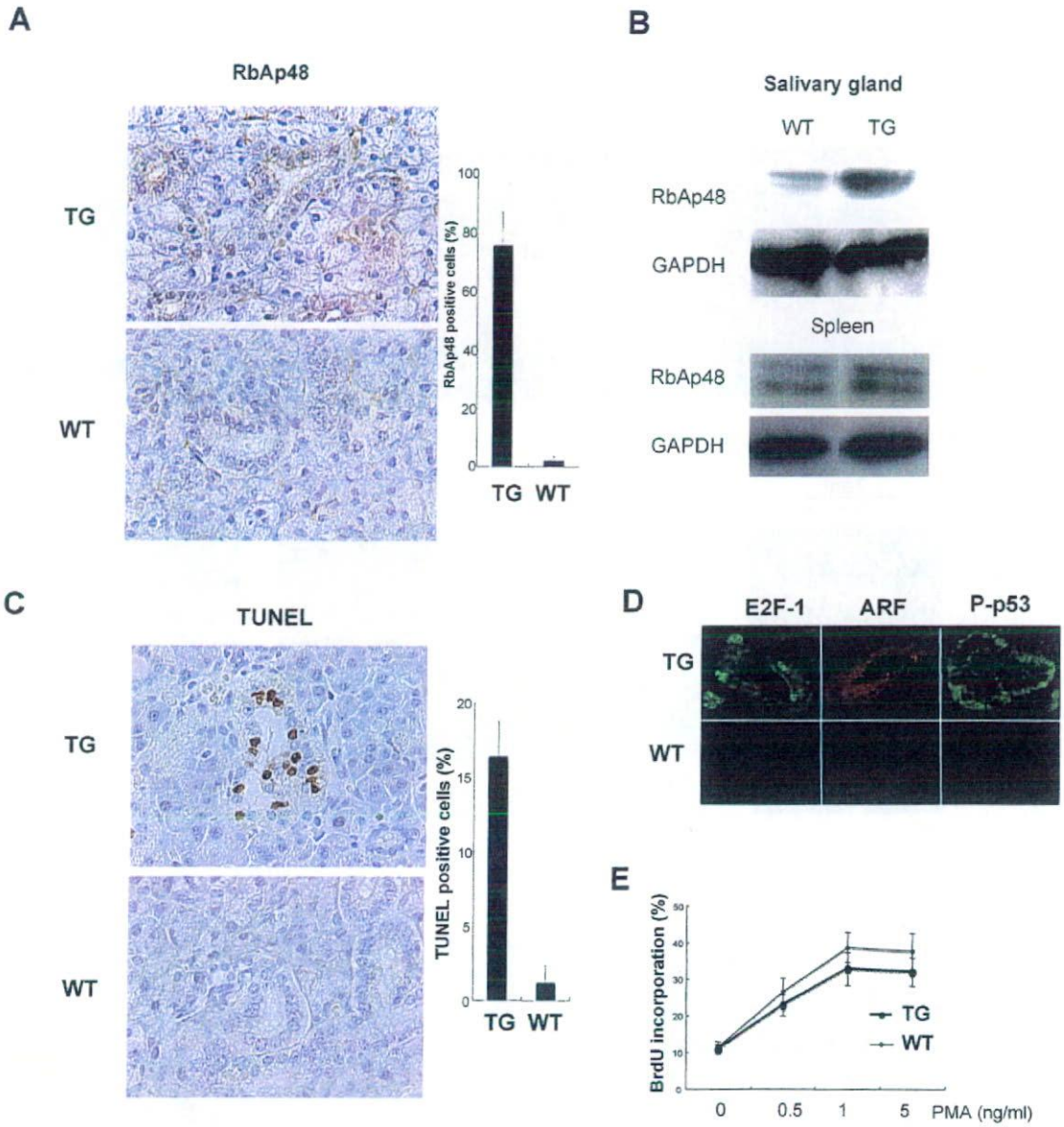

FIG. 6. RbAp48 overexpression and apoptosis in TG mice. (A) RbAp48 overexpression in the salivary gland tissues of TG mice but not WT mice at the age of 20 weeks detected by immunohistology. The percentage of RbAp48$^+$ cells was enumerated as described above (legend of Fig. 2B). (B) RbAp48 expression in the salivary gland tissues at the age of 20 weeks of TG mice compared with age-matched WT mice as detected by Western blotting. No differences in the levels of RbAp48 expression in spleens of WT and TG mice were detected. GAPDH expression was used for an internal control. (C) TUNEL$^+$ apoptotic epithelial duct cells were found in salivary glands of TG mice but not of age-matched WT mice at the age of 20 weeks. The percentage of TUNEL$^+$ cells was enumerated as described above. Images are representative of five mice. (D) Expression of E2F-1, p19ARF, and P-p53 was observed by confocal microscopy in the salivary glands of RbAp48-TG mice but not WT mice. Images are representative of five mice. (E) BrdU studies of TG mice with ectopic RbAp48 in the salivary glands demonstrated that cellular proliferation is barely affected. The graph is representative of three mice.

FIG. 5. RbAp48/E2F1/ARF-p53 pathway in the salivary glands. (A) Overexpression of RbAp48 in MSG cells from B6 mice induced E2F-1, p19ARF, and phospho-p53 (P-p53) expression, and the inhibitory effect of siRNA (15 nM) of RbAp48 was observed by confocal microscopic analysis. Cont, irrelevant siRNA control. Images are representative of three independent experiments. (B) TAM-induced apoptosis was associated with RbAp48 in MSG cells from B6 mice but not from ER$^{-/-}$, E2F1$^{-/-}$, and p53$^{-/-}$ mice as detected by confocal microscopy. Images are representative of two independent experiments. (C) Coexpression of RbAp48/E2F1, RbAp48/p19ARF, and RbAp48/p53 was detected by double-labeled confocal microscopic analysis in MSG cells of OVX B6 mice but not sham B6 mice. No differences in RbAp48/E2F1, RbAp48/p19ARF, and RbAp48/p53 expression levels were observed in MSG cells of non-OVX and OVX ER$^{-/-}$, E2F1$^{-/-}$, and p53$^{-/-}$ mice. Photos are representative of two independent experiments.

lacking many N- and C-terminal phosphorylation sites (36). These findings suggest that p53 phosphorylation is a key step in E2F-1-mediated apoptosis. The transcription factor E2F-1 functions as a key regulator for both cell cycle progression and apoptosis. E2F-2-deficient T lymphocytes exhibit enhanced T-cell receptor-stimulated proliferation and a lower activation threshold, leading to the accumulation of a population of autoreactive T lymphocytes, which appear to be responsible for causing autoimmunity in E2F-2-deficient mice (24). E2F-1$^{-/-}$ mice exhibit a defect in T lymphocyte development leading to an excess of mature T cells due to a maturation stage-specific defect in thymocyte apoptosis (8).

Our recent study suggests that antiestrogenic actions have a potent effect on the proteolysis of α-fodrin autoantigen in the salivary glands through upregulation of caspase 1 and caspase 3 activity (14). We found here a proteolysis of α-fodrin and a significant increase in caspase 3 activity in addition to the elevated caspase 1 and caspase 8 activity on RbAp48-induced apoptotic HSG cells. The fodrin α-subunit of various cells has been shown to be cleaved in association with apoptosis, in particular, due to upregulation of caspase 3 (4, 15, 48). Several reports have demonstrated that estrogen may play an inhibitory role in apoptosis in endothelial cells, breast cancer cells, cardiac myocytes, prostate cells, and neuronal cells (30, 32, 41, 43). Moreover, it has been noted that some enzymatic activities are elevated in postmenopausal women compared with normal healthy women (1, 27). Increased caspase levels seem to potentiate cell death in the presence of p53-generated signals that trigger caspase activation. Activated caspases digest many cellular proteins responsible for cell cycle regulation (e.g., Rb and Mdm2) (16), DNA damage recognition and repair [e.g., DNA-dependent protein kinase, p53, and poly(ADP-ribose) polymerase], and regulation of the cellular structure (e.g., actin, lamin, and fodrin) (44, 45). All these functional and structural protein modifications lead directly to apoptosis. Moreover, RbAp48 is found not only in histone deacetylase complexes but also in ATP-dependent remodeling complexes (9). Here we show that RbAp48 specifically activates E2F-1-mediated p53 phosphorylation in the salivary gland cells but not in many of the other types of cells examined. Thus, although the association of RbAp48 with nuclear transcriptional coactivators has not been described, there is abundant evidence that these histone binding factors interact with related classes of proteins (53, 46).

Taken together, our results demonstrate a direct molecular mechanism by which estrogen deficiency might promote p53-mediated apoptosis exclusively in exocrine gland cells through RbAp48 overexpression.

ACKNOWLEDGMENT

This work was supported in part by a Grant-in-Aid for Scientific Research (no. 17109016 and 17689049) from the Ministry of Education, Science and Culture of Japan.

REFERENCES

1. **Acarturk, F., and J. R. Robinson.** 1996. Vaginal permeability and enzymatic activity studies in normal and ovariectomized rabbits. Pharm. Res. **13:**779–783.
2. **Apostolou, I., Z. Hao, K. Rajewsky, and H. von Boehmer.** 2003. Effective destruction of Fas-deficient insulin-producing B cells in type 1 diabetes. J. Exp. Med. **198:**1103–1106.
3. **Christen, U., and M. G. Von Herrath.** 2002. Apoptosis of autoreactive CD8 lymphocytes as a potential mechanism for the abrogation of type 1 diabetes by islet-specific TNF-α expression at a time when the autoimmune process is already ongoing. Ann. N. Y. Acad. Sci. **958:**166–169.
4. **Cryns, V. L., L. Bergeron, H. Zhu, H. Li, and J. Yuan.** 1996. Specific cleavage of alpha-fodrin during Fas- and tumor necrosis factor-induced apoptosis is mediated by an interleukin-1beta-converting enzyme/Ced-3 protease distinct from the poly(ADP-ribose) polymerase protease. J. Biol. Chem. **271:**31277–31282.
5. **Ding, H. F., Y. L. Lin, G. McGill, P. Juo, H. Zhu, J. Blenis, J. Yuan, and D. E. Fisher.** 2000. Essential role for caspase-8 in transcription-independent apoptosis triggered by p53. J. Biol. Chem. **275:**38905–38911.
6. **Dou, Q. P., B. An, and P. L. Will.** 1995. Induction of a retinoblastoma phosphatase activity by anticancer drugs accompanies p53-independent G1 arrest and apoptosis. Proc. Natl. Acad. Sci. USA **92:**9019–9023.
7. **Enders, A., P. Bouillet, H. Puthalakath, Y. Xu, D. M. Tarlinton, and A. Strasser.** 2003. Loss of the proapoptotic BH3-only Bcl-2 family member Bim inhibits BCR stimulation-induced apoptosis and deletion of autoreactive B cells. J. Exp. Med. **198:**1119–1126.
8. **Field, S. J., F. Y. Tsai, F. Kuo, A. M. Zubiaga, W. G. Kaelin, Jr., D. M. Livingston, S. H. Orkin, and M. E. Greenberg.** 1996. E2F-1 functions in mice to promote apoptosis and suppress proliferation. Cell **85:**549–561.
9. **Gdula, D. A., R. Sandaltzopoulos, T. Tsukiyama, V. Ossipow, and C. Wu.** 1998. Inorganic pyrophosphatase is a component of the *Drosophila* nucleosome remodeling factor complex. Genes Dev. **12:**3206–3216.
10. **Haneji, N., T. Nakamura, K. Takio, K. Yanagi, H. Higashiyama, I. Saito, S. Noji, H. Sugino, and Y. Hayashi.** 1997. Identification of α-fodrin as a candidate autoantigen in primary Sjogren's syndrome. Science **276:**604–607.
11. **Hiebert, S. W.** 1993. Regions of the retinoblastoma gene product required for its interaction with the E2F transcription factor are necessary for E2 promoter repression and pRb-mediated growth suppression. Mol. Cell. Biol. **13:**3384–3391.
12. **Hugues, S, E. Mougneau, W. Ferlin, D. Jeske, P. Hofman, D. Homann, L. Beaudoin, C. Schrike, M. Von Herrath, A. Lehuen, and N. Glaichenhaus.** 2002. Tolerance to islet antigens and prevention from diabetes induced by limited apoptosis of pancreatic β cells. Immunity **16:**169–181.
13. **Ishimaru, N., K. Saegusa, K. Yanagi, N. Haneji, I. Saito, and Y. Hayashi.** 1999. Estrogen deficiency accelerates autoimmune exocrinopathy in murine Sjogren's syndrome through Fas-mediated apoptosis. Am. J. Pathol. **155:**173–181.
14. **Ishimaru, N., R. Arakaki, M. Watanabe, M. Kobayashi, K. Miyazaki, and Y. Hayashi.** 2003. Development of autoimmune exocrinopathy resembling Sjogren's syndrome in estrogen deficient mice of healthy background. Am. J. Pathol. **163:**1481–1490.
15. **Janicke, R. U., M. L. Sprengart, M. R. Wati, and A. G. Porter.** 1998. Caspase-3 is required for DNA fragmentation and morphological changes associated with apoptosis. J. Biol. Chem. **273:**9357–9360.
16. **Katsuda, K., M. Kataoka, F. Uno, T. Murakami, T. Kondo, J. A. Roth, N. Tanaka, and T. Fujiwara.** 2002. Activation of caspase-3 and cleavage of Rb are associated with p16-mediated apoptosis in human non-small cell lung cancer cells. Oncogene **21:**2108–2113.
17. **Kyprianou, N., H. F. English, N. E. Davidson, and J. T. Isaacs.** 1991. Programmed cell death during regression of the MCF-7 human breast cancer following estrogen ablation. Cancer Res. **51:**162–166.
18. **Lai, A., J. M. Lee, W. M. Yang, J. A. DeCaprio, W. G. Kaelin, Jr., E. Seto, and P. E. Branton.** 1999. RBP1 recruits both histone deacetylase-dependent and -independent repression activities to retinoblastoma family proteins. Mol. Cell. Biol. **19:**6632–6641.
19. **Lamhamedi-Cherradi, S. E., S. J. Zheng, K. A. Maguschak, J. Peschon, and Y. H. Chen.** 2003. Defective thymocyte apoptosis and accelerated autoimmune diseases in TRAIL$^{-/-}$ mice. Nat. Immunol. **4:**255–260.
20. **Lieman, J. H., L. A. Worley, and J. W. Harbour.** 2005. Loss of Rb-E2F repression results in caspase-8-mediated apoptosis through inactivation of focal adhesion kinase. J. Biol. Chem. **280:**10484–10490.
21. **Marchenko, N. D., A. Zaika, and U. M. Moll.** 2000. Death signal-induced localization of p53 protein to mitochondria. A potential role in apoptotic signaling. J. Biol. Chem. **275:**16202–16212.
22. **Mikkelsen, T. R., J. Brandt, H. J. Larsen, B. B. Larsen, K. Poulsen, J. Ingerslev, N. Din, and J. P. Hjorth.** 1992. Tissue-specific expression in the salivary glands of transgenic mice. Nucleic Acids Res. **20:**2249–2255.
23. **Miyagishi, M., and K. Taira.** 2002. U6 promoter-driven siRNAs with four uridine 3′ overhangs efficiently suppress targeted gene expression in mammalian cells. Nat. Biotechnol. **20:**497–500.
24. **Murga, M., O. Fernandez-Capetillo, S. J. Field, B. Moreno, L. R. Borlado, Y. Fujiwara, D. Balomenos, A. Vicario, A. C. Carrera, S. H. Orkin, M. E. Greenberg, and A. M. Zubiaga.** 2001. Mutation of E2F2 in mice causes enhanced T lymphocyte proliferation, leading to the development of autoimmunity. Immunity **15:**959–970.
25. **Nicolas, E., S. Ait-Si-Ali, and D. Trouche.** 2001. The histone deacetylase HDAC3 targets RbAp48 to the retinoblastoma protein. Nucleic Acids Res. **29:**3131–3136.
26. **Nicolas, E., V. Morales, L. Magnaghi-Jaulin, A. Harel-Bellan, H. Richard-Foy, and D. Trouche.** 2000. RbAp48 belongs to the histone deacetylase complex